Energy & Environmental Science

REVIEW

View Article Online
View Journal | View Issue

Cite this: *Energy Environ. Sci.*, 2014, **7**, 1850

Three-dimensional graphene materials: preparation, structures and application in supercapacitors

Xiehong Cao, Zongyou Yin and Hua Zhang*

Received 6th January 2014
Accepted 24th February 2014

DOI: 10.1039/c4ee00050a

www.rsc.org/ees

Three-dimensional (3D) graphene materials (3DGMs) are of great importance due to their unique properties and practical applications. A number of 3DGMs with novel structures have been developed in recent years. This review presents the current progress of 3DGMs. After introducing the preparation strategies of 3DGMs, we summarize the reported 3DGMs based on their different structures, and then focus on the description of their preparation methods, properties and applications. Lastly, the applications of 3D graphene-based materials in supercapacitors are described.

Broader context

In recent years, the assembly of graphene into macroscopic three-dimensional (3D) structures has been attracting intensive interest, because the utilization of 3D graphene materials (3DGMs) is one of the most effective ways to apply the unique properties of two-dimensional (2D) graphene nanosheets in practical applications. For example, the 3D porous graphene film not only facilitates the access of electrolyte to its surface, but also provides electrically conductive channels for the active materials anchored on it, leading to the enhanced performance of both electric double-layer capacitors and pesudocapacitors. Graphene fibers are highly flexible and easy to be functionalized, which makes them promising for flexible supercapacitors. Until now, a lot of effort has been devoted in order to control the morphologies and properties of 3DGMs, which are mainly aimed at obtaining 3DGMs with a porous structure, large surface area, good electrical conductivity, and high mechanical strength. 3DGMs can also be functionalized and integrated into devices easily, and are compatible with conventional material processing. This review paper summarizes various structures of 3DGMs together with their synthetic methods, properties and applications. In addition, the current challenge of the 3DGMs is also proposed.

1. Introduction

Graphene, a two-dimensional (2D) carbon sheet, has been used as one kind of promising material.[1] Due to its special structure, graphene possesses a lot of unique properties in chemistry, physics and mechanics.[2–4] Graphene has a carrier mobility up to 10 000 $cm^2 V^{-1} s^{-1}$ and a thermal conductivity of 3000–5000 W $m^{-1} K^{-1}$ at room temperature,[1,5] a high surface area of ~2630 $m^2 g^{-1}$,[6] good optical transparency of ~97.3% (ref. 7) and excellent mechanical strength with a Young's modulus of 1.0 TPa.[8] Various synthetic methods of graphene including mechanical cleavage,[1] epitaxial growth,[9] graphitization,[10] exfoliation[11] and chemical vapor deposition (CVD)[12,13] have been developed in the past few years, which have promoted the intensive study of graphene-based materials in numerous research areas, such as electronics,[14–22] energy storage applications,[23–28] sensors[29–36] and so on.

Recently, three-dimensional (3D) graphene materials (3DGMs) have been attracting much attention, since they not only possess the intrinsic properties of 2D graphene sheets, but also provide advanced functions with improved performance in various applications.[37–42] In particular, due to their unique mechanical characteristics, excellent electrical conductivity and large surface area, 3DGMs have emerged as promising candidates for supercapacitors.[43–45]

Massive production of graphene sheets is of great importance for the fabrication of 3DGMs. The method involving preparation of graphene oxide (GO) followed by a reduction process is the most common way to obtain graphene materials.[11] Although the resultant reduced graphene oxide (rGO) sheets contain defects and exhibit low electrical conductivity, the advantages of high throughput and low cost of this method make GO and rGO favorable as building blocks for the fabrication of graphene-based materials.[3,46–55] Alternatively, the chemical vapor deposition (CVD) method is an effective way to produce graphene of a high quality, similar to that of pristine graphene.[12,13] Recently, a 30 inch graphene film has been prepared through the CVD method, indicating the potential of large-scale production of graphene through this method.[56]

To date, a number of synthetic methods for 3DGMs, based on the strategies of either self-assembly, template-assisted preparation or direct deposition, have been developed in recent years. Numerous 3DGMs with various structures and unique functions have emerged. In this review, we mainly focus on the

School of Materials Science and Engineering, Nanyang Technological University, 50 Nanyang Avenue, Singapore 639798, Singapore. E-mail: HZhang@ntu.edu.sg; Web: http://www.ntu.edu.sg/home/hzhang/

description of the structures of 3DGMs, and then introduce their preparation methods and properties. Moreover, the supercapacitor application of 3D graphene-based materials is also reviewed.

2. Preparation methods

In the past few years, tremendous efforts have been devoted to the development of synthetic methods for 3DGMs with various morphologies, structures and properties, in order to satisfy the requirements arising from different applications. In this section, the preparation methods are generally classified as self-assembly, template-assisted preparation and direct deposition.

2.1. Self-assembly

Self-assembly is one of the most commonly used strategies to obtain 3DGMs. A lot of methods based on this strategy have been developed. As a typical example, 3D graphene structures can be produced through the gelation process of GO dispersion followed by reduction to convert GO to rGO.[57] In a stable GO dispersion, there is a force balance between the van der Waals attractions from the basal planes of GO sheets and the electrostatic repulsions from the functional groups of GO sheets, which makes GO sheets well dispersed in an aqueous solvent. Gelation of the GO dispersion occurs once the force balance is broken. During the gelation process, GO sheets partially overlap to form GO hydrogels with 3D architectures. After further reduction of the GO hydrogels, 3D rGO networks are obtained. There are many ways to trigger the gelation of a GO dispersion, such as addition of cross-linkers,[58] changing the pH value of the GO dispersion,[57] or ultrasonication of the GO dispersion.[59] Polyvinyl alcohol (PVA) is a cross-linker first reported by Shi *et al.*, which can enhance the attraction of GO sheets and promote the gelation process of a GO dispersion.[58] Moreover, a lot of other materials have also been used as the cross-linkers for the self-assembly of GO sheets, such as DNA,[60] metal ions,[61–63] polymers,[64] organic molecules,[65] and so on. Besides the methods based on the gelation process of a GO dispersion, the self-assembly of GO sheets into 3D structures has also been achieved by other methods, such as direct freeze-drying,[66] tape casting,[67] controlled filtration[68] and centrifugation of GO dispersions,[69] electrochemical deposition,[70] sol–gel reaction,[71,72] and so on. Alternatively, 3D rGO architectures can be directly obtained through the hydrothermal[73–80] or chemical[81] reductions of GO sheets. In these cases, GO sheets are self-assembled to form 3D networks, and at the same time converted to rGO.

2.2. Template-assisted preparation

Compared with the self-assembly methods, by using pre-designed 3D templates, 3DGMs with much more controlled morphologies and properties can be obtained. This strategy has been well demonstrated by the direct growth of graphene on 3D templates using CVD methods.[37,40,82] For example, by using

Xiehong Cao received his B.E. in the Department of Polymer Materials and Engineering in Zhejiang University, China (2008). He completed his PhD under the supervision of Prof. Hua Zhang in the School of Materials Science and Engineering of Nanyang Technological University, Singapore (2012). He is currently working as a Research Fellow in Prof. Hua Zhang's group. His research interests include the synthesis, characterization and applications of two-dimensional nanomaterials.

*Zongyou Yin studied at Jilin University in China for his B.E. and M.S., and completed his PhD at Nanyang Technological University in Singapore (2008). He joined Prof. Hua Zhang's group in 2008 as a Postdoctoral Fellow, and then worked as a Scientist II in Institute of Materials Research and Engineering at A*STAR of Singapore in 2013. He is currently a Postdoctoral Associate in Massachusetts Institute of Technology in USA. His research interests include the synthesis of low-dimensional nanomaterials and their applications in energy, environment and optoelectronics.*

Prof. Hua Zhang obtained his B.S. and M.S. from Nanjing University in 1992 and 1995, respectively, and completed his PhD with Prof. Zhongfan Liu at Peking University in 1998. As a Postdoctoral Fellow, he joined Prof. Frans C. De Schryver's group at Katholieke Universiteit Leuven (Belgium) in 1999, and then Prof. Chad A. Mirkin's group at Northwestern University in 2001. After working at NanoInk Inc. (USA) and Institute of Bioengineering and Nanotechnology (Singapore), he joined Nanyang Technological University in July 2006. His current research interests focus on two-dimensional nanomaterials including graphene and metal dichalcogenides, and their applications in nano- and bio-sensors, clean energy, water, environment, etc.

commercially available Ni foam as both the template and catalyst, 3D graphene networks (3DGNs) were successfully synthesized.[37,40] Moreover, anodic aluminum oxide (AAO),[83] MgO,[84] nickel-coated pyrolyzed photoresist films,[85,86] metal nanostructures[82,87,88] and even metallic salts[38,89] have also been used as templates to produce 3DGMs. Compared to the conventional CVD process, which uses flat metal substrates as templates and normally produces a limited amount of graphene, large-amounts of graphene materials can be achieved by using 3D templates. This greatly benefits the applications that require a large quantity of graphene.

Alternatively, 3D graphene architectures can be obtained in another convenient way *via* the assembly of GO sheets onto 3D templates followed by the reduction of GO to rGO. Many assembly techniques have been developed, such as electrophoretic deposition,[90] dip-coating,[91] refluxing in an autoclave[92,93] and template-assisted freeze-drying.[94] The templates used in these methods are not limited to metal substrates; non-metals including silica nanoparticles (NPs),[95–97] polystyrene (PS) balls,[44,98–100] Nafion scaffolds,[101] commercially available sponges,[102,103] cellulose[104] and textile fibers[105] have also been reported.

2.3. Direct deposition

As a straightforward strategy, the direct deposition of 3D graphene architectures on conductive substrates, *e.g.* Au and stainless steel, has been demonstrated by plasma-enhanced CVD (PECVD) methods.[42,106–108] The graphene sheets were vertically grown on the substrate and connected with each other to form 3D porous graphene, which firmly adhered to the substrate. Importantly, the numerous active sites at the edges of the vertical graphene sheets make this 3D graphene suitable for sensing applications. For example, Chen *et al.* fabricated a biosensor, composed of graphene sheets vertically grown on a gold electrode and Au NP–antibody conjugates, that could provide a low detection limit of $\sim$2 ng mL^{-1} of immunoglobulin G.[42] In addition, the placement of 3DGMs can also be easily controlled by patterning the metal substrate with designed features, which might enable construction of various sensor structures for different applications.[107]

3. Structures

Benefiting from the rapid development of preparation methods in previous years, a number of 3DGMs with different structures, morphologies and properties have been prepared. In addition, these 3DGMs have also shown promising applications in many areas. Table 1 summarizes the most typical structures of 3DGMs, along with their preparation methods, properties and applications.

3.1. 3D graphene networks (3DGNs)

3DGNs, including graphene foams,[41,96,109] sponges,[102,110] hydrogels[111,112] and aerogels,[66,78,94] are one of the most reported 3D graphene structures, which have shown promising properties for numerous applications. As an example, Yu *et al.* utilized commercially available polyurethane sponge (PU) as a template, and fabricated a 3D rGO–PU sponge based on a simple dip-coating method.[102] This rGO–PU sponge showed high sensitivity to the pressure applied on it, which was able to detect a minimum pressure of 9 Pa, making it promising as a flexible and sensitive pressure sensor. As shown in Fig. 1a and b, the artificial skin, which was made of a rGO–PU sponge covered by electrode arrays, was able to measure the spatial distribution of pressure applied on it. In addition, 3D rGO networks were also obtained by electrochemical methods, in which GO sheets were electrochemically reduced and then deposited on the electrodes.[70,113]

Although many methods have been developed to prepare 3D rGO networks, the resultant materials normally were of low quality and exhibited poor electrical conductivity. Recently, other approaches, including the CVD method, have been reported for preparing high-quality 3DGNs. In a typical CVD process, graphene is deposited on the surface of metal substrates, *e.g.* commonly used Cu or Ni films or foils,[12,13] where the metal substrates serve as both catalysts and templates. Therefore, it is reasonable to think that 3D graphene architectures can be prepared in the CVD process by using pre-fabricated 3D metal substrates as templates. Since a 3D metal substrate has a larger surface area compared to a flat metal substrate, a higher amount of graphene is expected for the same growth time. Recently, Ni foam with a pore size of several hundred micrometers, commonly used as the current collector in energy storage applications, has been successfully used as the template for preparation of 3DGNs through the CVD method.[37,40] The D-band, a characteristic peak of graphene related to the density of disordered carbon,[114] was negligible in the Raman spectra of 3DGNs, indicating the high quality of the obtained graphene film.[37,40] The surface area of 3DGNs is dependent on the layer number of the graphene film, which is as high as $\sim$850 m^2 g^{-1} for 3DGNs composed of a 3-layer graphene film.[37] Importantly, the 3DGNs have also exhibited unique properties in electrical conductivity,[37] mechanical strength[37,115,116] and thermal conductivity.[117] Our work also showed 3DGNs of $\sim$0.1 g per batch can be achieved in an atmospheric pressure CVD process using ethanol as the carbon source,[40] indicating the potential for massive production of CVD-synthesized, high-quality graphene material at low cost. Until now, a number of graphene composites based on 3DGNs have been also demonstrated, which were fabricated through various methods such as hydrothermal,[118,119] electrochemical deposition,[120] CVD[121,122] and so on. These 3DGN-based composites have shown superior properties and performance in various applications including supercapacitors,[40,118,119,123] sensors,[120,124] batteries,[115,121,125–127] hydrogen evolution reaction (HER),[128] oxygen reduction reaction (ORR),[129] electromagnetic interference shielding,[116] light-emitting diodes (LED),[130] solar cells,[131] and cell cultures.[132]

Using Ni foam as a template in the CVD process is an effective way to produce 3DGMs with a controlled morphology. However, the obtained products possessed large pore sizes (hundreds of micrometers) with high porosity ($\sim$99.7%).[37] To further reduce the pore size and increase the yield of graphene, other templates have been explored. For example, by using commercially available Ni NPs below 30 μm in size as the

Table 1 Comparison of various structures of 3D graphene materials with their preparation methods, properties and applications

Structures	Synthetic methods	Properties	Applications	Ref.
3D graphene networks	CVD using $NiCl_2 \cdot 6H_2O$ as catalyst precursor	Surface area: ~560 $m^2 g^{-1}$, electrical conductivity: ~12 S cm^{-1}	Absorbent	38
	CVD based on Ni foam template	Surface area: ~850 $m^2 g^{-1}$, electrical conductivity: 10 S cm^{-1}, tensile strain: ~95%		37
	Self-assembly of GO sheets induced by hydrothermal reaction	Electrical conductivity: ~0.0025 S cm^{-1}, compressive strength: ~0.042 MPa, compression modulus: ~0.26 MPa	Catalysis	74
Graphene fibers	Wet-spinning	Surface area: ~884 $m^2 g^{-1}$, electrical conductivity: 2600–4900 S cm^{-1}, specific tensile strength: 188 kN m kg^{-1}, compression modulus: 3.3 MPa	Conductive wire	166
	Wet-spinning	Electrical conductivity: 8–10 S cm^{-1}, tensile strength: 140–150 MPa	Micro-pump	168
	Wet-spinning	Electrical conductivity: ~35 S cm^{-1}, tensile strength: ~182 MPa, Young's modulus: 8.7 GPa	Conductive wire	164
Graphene tubes	Hydrothermal using Cu wire as template	Electrical conductivity: 10 S cm^{-1}, tensile strength: ~180 MPa	Self-powered micromotor	173
	CVD using AAO as template	Electrical conductivity: 950 S m^{-1}, thermal conductivity: 8.28 W m^{-1} K^{-1}	Heat transfer and thermal energy storage	83
3D porous graphene films	Leavening strategy	Sheet resistance: <100 Ω sq^{-1}, tensile strength: ~3.2 MPa	Supercapacitor	45
	Assembly of chemically modified graphene using PS particles as template	Surface area: 194.2 $m^2 g^{-1}$, electrical conductivity: 1024 S cm^{-1}	Supercapacitor	100
Graphene balls	Aerosol-assisted capillary compression process	Surface area: 82 $m^2 g^{-1}$, compression strength: >55 MPa	Microbial fuel cell	177
	CVD using PS ball as template	Surface area: 508 $m^2 g^{-1}$, electrical conductivity: 6.5 S m^{-1}	Supercapacitor	44
Honeycomb-like 3D graphenes	Freeze-casting	Electrical conductivity: ~0.12 S m^{-1}, compression strength: ~8 kPa (plateau state), 18 kPa (80% strain), for sample with density of 5.1 mg cm^{-3}		184
	Self-assembly	Electrical conductivity: 649 S m^{-1}	Supercapacitor	197

template, 3DGNs were obtained.[82] During the annealing process at high temperature, Ni NPs were melted and agglomerated together to form a 3D Ni template. The yield of the obtained graphene was ~2.5% of the weight of the Ni NPs used. Lee *et al.* further simplified the CVD process for synthesis of 3DGNs by annealing a mixture of Ni powder and poly(methyl methacrylate) (PMMA) at low pressure.[133] PMMA has already been demonstrated as an effective solid carbon source for the preparation of graphene on flat metal substrates.[134] Compared to common gaseous carbon sources, *e.g.* CH_4, the use of PMMA makes the CVD process cheaper and safer. In addition, the instrument setup is also simplified due to removal of the corresponding gas lines and accessories of the CVD system. The yield of graphene in Lee *et al.*'s work was 0.5 g if 20 g Ni powder was used.

Recently, a nickel salt ($NiCl_2 \cdot 6H_2O$) was also used as both the catalyst precursor and template for 3DGNs.[38] During the annealing of $NiCl_2 \cdot 6H_2O$ under a mixture of H_2–Ar gas at 600 °C, a mixture of gas containing water vapor and hydrogen chloride (product of the reaction between $NiCl_2$ and H_2) was

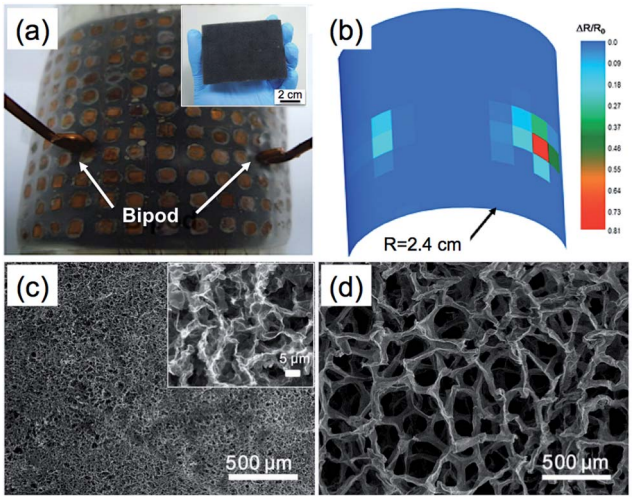

Fig. 1 (a) Photograph of the artificial skin made from a rGO–PU sponge. Inset: photograph of the rGO–PU sponge. (b) The mapping profile of resistance change of the rGO–PU sponge in (a), which was caused by pressing the bipod (70 g). Reproduced with permission from ref. 102, copyright 2013, WILEY-VCH Verlag GmbH & Co. KGaA. (c and d) Comparison of the 3DGMs obtained by using templates of $NiCl_2 \cdot 6H_2O$ (c) and Ni foam (d). Inset in (c): high-magnification SEM image of the 3DGM in (c). Reproduced by permission from Macmillan Publishers Ltd: ref. 38, copyright 2013.

rapidly released, resulting in the formation of a 3D Ni skeleton. After the subsequent CVD process operated at 1000 °C followed by etching of Ni, a 3D graphene macroscopic object (3D-GMO) was obtained (Fig. 1c). As shown in Fig. 1c and d, the pore size of the 3D-GMO (several micrometers) was much smaller than that of the 3DGN obtained from Ni foam (several hundred micrometers).[38] The smaller pore size also resulted in a relatively higher density of 3D-GMO ranging from ~22 to ~100 mg cm^{-3}, compared with that of 3DGN (~1 mg cm^{-3}).[38] Due to a high surface area (~560 m^2 g^{-1}), the 3D-GMO showed excellent performance in the removal of heavy metal ions.

Alternatively, 3DGNs can also be obtained by microwave irradiation of graphite powders,[135] or the direct graphitization process of some carbon-containing substances, such as resin[136] and sugar.[137]

3.2. 3D porous graphene films

Due to the π–π stacking interaction and van der Waals attraction among their basal planes, GO or rGO sheets tend to stack in a graphitic structure, leading to significant loss of their surface area. The restacking and aggregation of GO or rGO sheets also hamper the large-scale usage and process of graphene materials in many applications, especially energy storage devices,[138] because it is difficult for electrolyte ions to access the interspace among the densely packed graphene sheets.

To solve this problem, fabrication of a 3D porous graphene film by the incorporation of spacer materials between the graphene sheets is an effective way to retain the surface area of the graphene. The spacer materials can be carbon nanomaterials,[139–141] nanodiamond,[142] polymers,[21,143] noble metal nanocrystals,[144,145] metal oxides,[54,146] mesoporous silica sheet,[147] metal organic frameworks (MOF)[148] and so on. Moreover, water molecules were also reported by Li *et al.* as a spacer material for enlarged interspacing between stacked chemically converted graphene (CCG) sheets.[68] Although the obtained graphene film contained over 92 wt% water, it still exhibited high electrical conductivity with a sheet resistivity of 1860 Ω sq^{-1}. This is because the CCG sheets in the wet film still have a nearly face-to-face-stacked morphology, which ensures the effective electron transport paths presented in the graphene film. Their recent work showed that non-volatile liquids can also act as spacer materials.[149] In their work, the wet CCG film prepared by a filtration method was placed in a mixture containing volatile and non-volatile liquids, *e.g.* H_2O–H_2SO_4. After the water in the CCG film was completely exchanged by the mixture, the film was placed in a vacuum oven to evaporate the volatile solvent, and the remaining non-volatile liquid prevented the restacking of the CCG sheets. The packing density of the CCG film was also increased after evaporation of the volatile liquid. Compared with the other porous graphene films with a packing density of 0.05–0.75 g cm^{-3},[150,151] the graphene film obtained by Li *et al.* showed a higher value of ~1.33 g cm^{-3}. Importantly, the used non-volatile liquids, *e.g.* H_2SO_4 and 1-ethyl-3-methylimidazolium tetrafluoroborate (EMIMBF4), can serve as electrolytes, which enables the direct integration of the obtained graphene films into supercapacitor devices.

Other methods without the use of spacer materials, such as tap casting,[67] light scribing,[152,153] leavening,[45] and chemical activation,[154–156] through treatments of GO/rGO films have also been reported to fabricate 3D porous graphene films. In a recent work, Chen *et al.* used a so-called "leavening" strategy, similar to the process of baking bread, to fabricate a porous rGO film, in which the compacted GO film acted as the "dough".[45] After the GO film was first prepared by filtration of a GO dispersion through an AAO membrane, it was peeled off from the AAO membrane and then placed in an autoclave with hydrazine at 90 °C for 10 h. During this process, numerous pores were formed in the rGO film, which was attributed to the rapid release of gaseous species, due to reduction of GO, from the compact film. Because of its porous structure and the hydrophobic nature of rGO, the resultant rGO film exhibited an improved absorption ability to organic solvents, such as motor oil and petroleum, compared with the compact rGO film and graphite.[45]

Recently, 3D porous graphene films have also been fabricated using PS nanospheres,[100,157] silica particles,[95] or PMMA spheres[158] as templates. For example, the porous chemically modified graphene (CMG) film with a uniform pore size of ~2 μm was obtained by filtration of an aqueous mixture of PS nanospheres and CMG sheets followed by the removal of PS (Fig. 2).[100] The resultant porous film possessed a high electrical conductivity of 1204 S m^{-1} and a surface area of 194.2 m^2 g^{-1}, which was subsequently functionalized with MnO_2 and then used as a supercapacitor electrode.

3.3. Graphene fibers

In previous years, carbon fibers with high mechanical strength and electrical conductivity have been successfully fabricated by

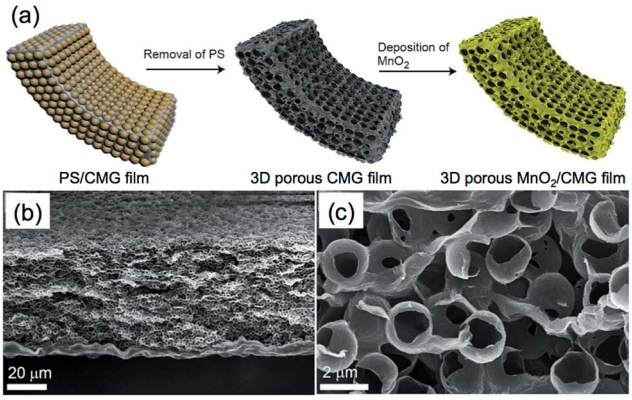

Fig. 2 (a) Schematic illustration of the synthesis process of 3D porous MnO_2/CMG composite film. (b) Low- and (c) high-magnification cross-section SEM images of the obtained 3D porous CMG film. Reproduced with permission from ref. 100. Copyright 2012, American Chemical Society.

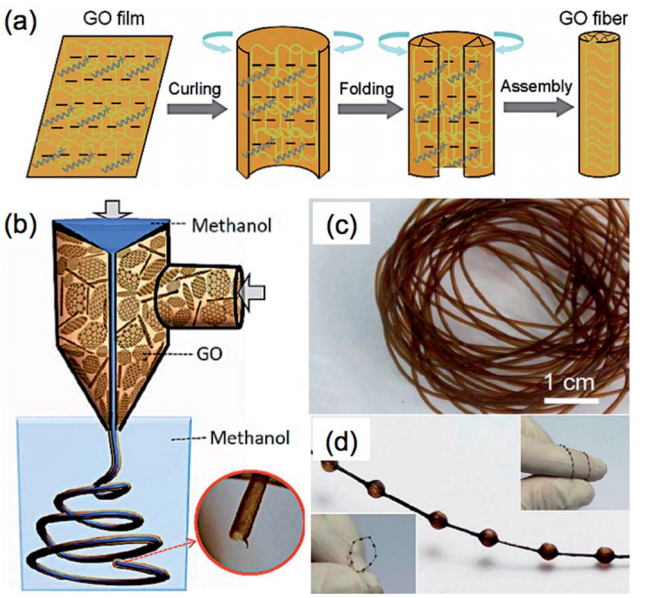

Fig. 3 (a) Schematic illustration of the formation mechanism of GFs. Reproduced by permission from Macmillan Publishers Ltd: ref. 164, copyright 2012. (b) Schematic illustration of the fabrication process of GO hollow fibers (GO-HFs). (c and d) Photographs of the obtained GO-HFs (c) and necklace-like fibers (d). Reproduced with permission from ref. 168. Copyright 2013, American Chemical Society.

assembling carbon nanotubes (CNTs), which have shown great importance in industry and our daily life.[159–161] The mechanical, electrical and thermal properties of graphene are superior to that of other carbon materials,[1,5,8] suggesting that the fabrication of graphene-based carbon fibers would provide more advantages in the practical applications of carbon fiber materials. In comparison with conventional carbon fibers, graphene fibers (GFs) not only exhibit the ordinary features of carbon fibers such as flexibility and electrical conductivity, but also possess unique properties such as lightweight, facile functionalization and low cost. GFs also exhibited a much lower density ($\sim$0.23 g cm^{-3}) compared with conventional carbon fibers (>1.7 g cm^{-3}) and metal wires ($\sim$20 g cm^{-3}).[43] The diameter of GFs is normally in the micrometer range, while the length can be up to several tens of centimeters, which gives GFs a high aspect ratio (>10 000).

The current methods for the preparation of GFs are mainly based on the strategy of controlled assembly of GO sheets,[43,162–169] such as hydrothermal treatment of a GO dispersion in a confined container[165] and wet-spinning of a concentrated GO liquid crystal.[163] Recently, the Yu group developed a method *via* injection of a GO dispersion into cetyltrimethylammonium bromide (CTAB) solution, leading to the self-assembly of GO sheets into a fiber-like structure.[164] The formation of GFs followed the "curliness-fold" formation mechanism, in which the positively-charged CTAB molecules played an essential role (Fig. 3a). After the adsorption of CTAB molecules on the negatively-charged surface of GO sheet, the electrostatic repulsion among the GO sheets was reduced, leading to the curling and folding of the GO sheets. The GO fibers were obtained after continuous adsorption of CTAB molecules on the GO sheets and repeating the process of curling and folding of GO sheets. The resultant GFs had a long length of $\sim$1.6 m, and also possessed good mechanical strength ($\sim$182 MPa), high electronic conductivity ($\sim$35 S cm^{-1}), and flexibility. Functionalizations of the GFs by polymers or CNTs were also achieved, which further enhanced the mechanical strength of the GFs and also extended the applications of GF-based materials. For example, the GF composited with poly(*N*-isopropylacrylamide) (PNIPAM) was used as a thermosensitive device.[164]

Similar to the aforementioned Yu's method,[164] hollow GFs have been fabricated by Qu *et al.*, in which a coaxial two-capillary spinneret was used to simultaneously inject the GO suspension and methanol into the coagulation bath.[168] The obtained GO hollow fibers (GO-HFs) showed a pipe-like morphology with a large diameter of $\sim$700 μm (Fig. 3b and c), and exhibited a tensile strength of $\sim$140 MPa. After reduction of the GO-HFs, the resultant rGO-HFs had an electrical conductivity of 8–10 S cm^{-1}. It is worth mentioning that formation of the GO-HFs was very fast. It only took 30 s to produce 1 meter length GO-HFs. Interestingly, necklace-like fibers were also obtained (Fig. 3d), which may have a potential application in a micro pump.[168]

A GF with a unique core–shell structure, in which the core was composed of porous graphene film and the shell was made of densely stacked graphene sheets, was achieved by Gao *et al.*[166] To prepare this "porous core@dense shell" GF, GO liquid crystals were firstly flowed through a capillary tube and injected into liquid nitrogen, then subjected to freeze-drying and reduction processes. Due to its unique structure, the GF not only exhibited high porosity with a specific surface area as high as 884 m^2 g^{-1}, but also possessed excellent electrical conductivity and mechanical strength. Attributed to its densely packed shell, the GF exhibited an electrical conductivity of 2.6×10^3 S m^{-1}, which can be increased further to 4.9×10^3 S m^{-1} after an annealing treatment, which is much higher than that of

graphene aerogels.[72,73] The porous core of this GF also enabled the fabrication of GF-based composites, since the additives can be readily infiltrated into the pores. GFs composited with a polymer, Ag and Pt nanocrystals have been demonstrated, which might be promising in catalysis and energy storage.[166]

The preparation method of GFs is not limited to the assembly of GO sheets; GF can also be fabricated using CVD-produced graphene through a simple "drawing" method.[170] After etching of the metal template, the graphene film was first floated on the surface of a mixture of ethanol and water, and subsequently drawn out by tweezers. After evaporation of the solvents, GF with a porous structure was obtained. Benefiting from the use of a high-quality graphene film produced by the CVD method, this GF possessed a high electrical conductivity of ~1000 S m^{-1}.

3.4. Graphene tubes

Materials with tube-like structures have exhibited great potential as vessels in applications such as separation, purification and fluidics.[171,172] Graphene tubes show a similar morphology to that of CNTs but possess a larger inner diameter. This makes functionalization of the inner wall of a graphene tube much easier. Moreover, the walls of graphene tubes are composed of stacked graphene layers, which endow the graphene tube with high electrical conductivity and excellent mechanical strength.

Templates are normally required to prepare graphene tubes.[83,87,109,173] For example, Wang *et al.* used Ni nanowires with a diameter of ~70 nm as both the catalyst and template for the synthesis of graphene tubes by the CVD method.[87] The Ni nanowires were prepared by electrodeposition of Ni into an anodic aluminum oxide (AAO) membrane followed by etching of the AAO. To prepare the graphene tubes, a CVD process was first operated to deposit graphene on the surface of Ni nanowires. Graphene tubes were obtained after etching of Ni by 1 mol L^{-1} $FeCl_3$, and these tubes exhibited a similar diameter to that of Ni nanowires. Recently, graphene was also successfully grown on the inner walls of the pores of an AAO membrane in a CVD process.[83] The obtained graphene exhibited a tube-like structure with good thermal transport properties. In a recent work by Qu *et al.*, graphene microtubings (μGTs) were fabricated based on the template of Cu wires through the hydrothermal method.[173] In this method, Cu wires were placed inside a glass pipeline followed by filling of the pipeline with a GO dispersion (Fig. 4a). The GO sheets were aggregated and wrapped around the Cu wires after the hydrothermal reduction. The μGTs were obtained after removal of the Cu wires and pipeline. Interestingly, by choosing the glass pipeline and the Cu wire with the proper size and shape, it was possible to easily control the shape and diameter of the prepared μGTs. For instance, a μGT spring can be obtained by wrapping the wet μGT around a rod before drying (Fig. 4b). Helical and multi-channel μGTs can also be readily fabricated by twisting two Cu wires and inserting several Cu wires together into the glass pipeline, respectively, prior to the hydrothermal treatment (Fig. 4c and d). The μGTs showed a tensile strength of up to 180 MPa, which is comparable to that of the solid GFs.[162,163] Importantly, selective

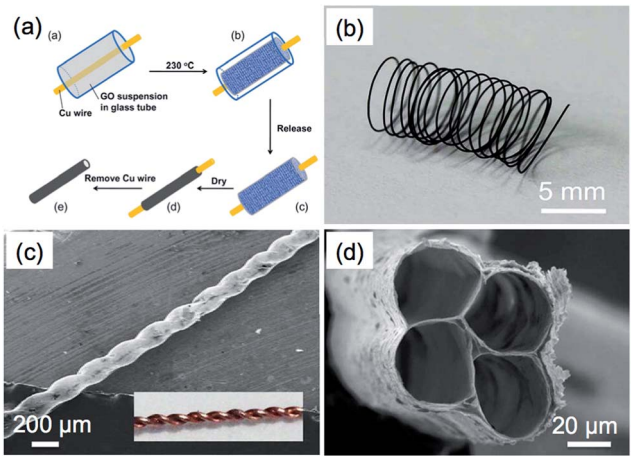

Fig. 4 (a) Schematic illustration of the fabrication process of graphene microtubings (μGTs). (b) Photograph of a μGT spring. (c) SEM image of a helical μGT fabricated based on a twist of two Cu wires (inset). (d) SEM image of a 4-channel μGT. Reproduced with permission from ref. 173. Copyright 2012, American Chemical Society.

functionalization of the outer-wall and inner-wall of the μGTs could also be achieved, which made the μGTs suitable for a wide range of applications. As an example, the μGT decorated with Pt NPs on its inner wall was used as a self-powered micromotor, which might be useful in the application of drug delivery.[173] In addition to the aforementioned methods, a recent report showed that graphene tubes can also be obtained by partially unzipping the carbon nanofiber along its longitudinal axis.[174]

3.5. Graphene spheres

Graphene spheres (GSs), which normally possess a structure of hollow spheres with a shell of stacked graphene layers, have found promising applications in oil absorption,[98] supercapacitors,[39,44] and lithium ion batteries.[175]

GSs were mainly prepared based on spherical templates such as metal NPs.[88,176] For example, Choi *et al.* reported the synthesis of hollow GSs *via* thermal annealing of triethylene glycol (TEG)-coated Ni NPs.[88] The synthesis of GSs involve three steps. First, the Ni NPs coated with TEG were annealed at 250 °C to decompose the TEG molecules to carbon atoms. Then the Ni NPs were subjected to another annealing at 500 °C under an argon atmosphere, which led to the transformation of these adsorbed carbon atoms to graphene layers. After removal of Ni by HCl, the GSs with a similar diameter to that of the Ni NP template were obtained without collapse of the structure. Using pre-synthesized Ni NPs and the relatively low-temperature annealing process at 500 °C, it makes this synthetic process simple and scalable.

In addition, it is cheaper and more convenient to use metal salts instead of metals as the templates for the synthesis of GSs.[44,89] As an interesting example, a nano-frame graphene structure (3D-NFG) was obtained using $NiCl_2$ as a catalyst and polyvinyl alcohol (PVA) as a solid carbon source through a CVD process.[89] The prepared GSs were interconnected with few-layer graphene sheets, which exhibited a low sheet resistance of ~700

Ω sq^{-1}. The resultant 3D-NFG could be used as an alternative counter electrode of Pt for dye sensitized solar cells (DSSC). Recently, graphene nanoballs with meso-pores (MGBs) were achieved in a precursor-assisted CVD process using $FeCl_3$ and PS balls as the catalyst precursor and carbon source, respectively (Fig. 5a–d).[44] The obtained MGBs possessed a high specific surface area of 508 m^2 g^{-1} and average pore size of ~4.27 nm. To prepare the MGBs, the PS balls were first functionalized with –COOH and –SO_3H groups to achieve a good dispersion of PS balls in $FeCl_3$ aqueous solution. Then the PS balls were annealed at 1000 °C under a H_2–Ar atmosphere. During this process, 3D iron nanoframes were formed, arising from the aggregation of these iron ions adsorbed on the surface of PS balls. Meanwhile, PS balls were decomposed and served as a solid carbon source for the growth of graphene on 3D iron nanoframes. After removal of the iron by HCl, MGBs were obtained.

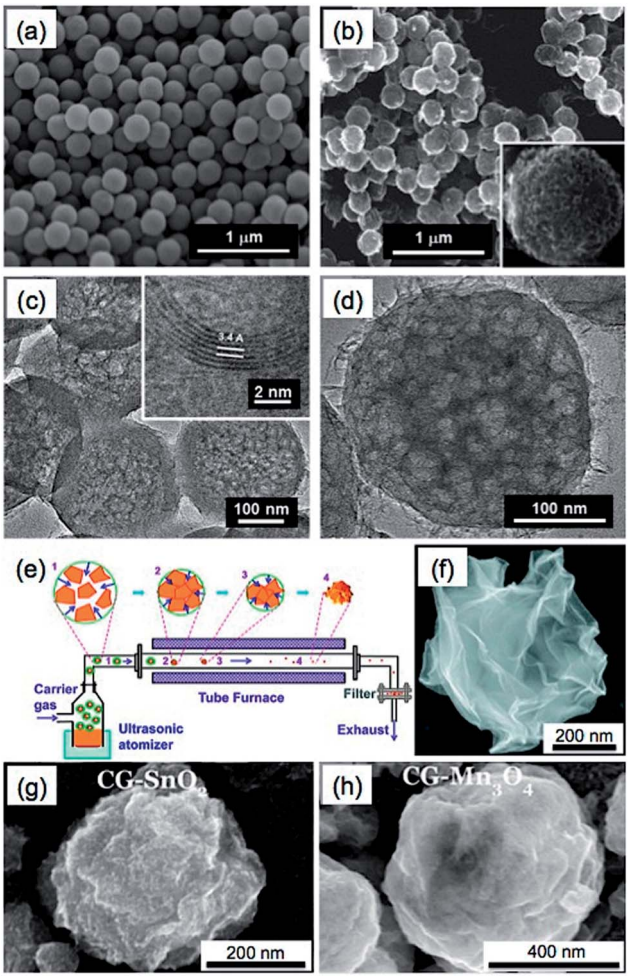

Fig. 5 SEM images of (a) the PS balls functionalized with –COOH and –SO_3H groups and (b) the graphene nanoballs with meso-pores (MGBs). Inset in (b): high-magnification SEM image of a MGB. (c and d) TEM images of MGBs. Inset in (c): high-resolution TEM image of a MGB shows an interlayer spacing of 0.34 nm. Reproduced with permission from ref. 44. Copyright 2013, American Chemical Society. (e) Schematic illustration of the synthetic process of paper-ball-like GS. (f) SEM image of a GS. Reproduced with permission from ref. 177. Copyright 2011, American Chemical Society. (g and h) SEM images of the crumpled graphene (CG) balls composited with SnO_2 (g) and Mn_3O_4 (h). Reproduced with permission from ref. 39. Copyright 2012, American Chemical Society.

In addition to the CVD methods, GSs have been also prepared by directly assembling GO sheets into spherical structures.[39,98,177–181] Through use of an aerosol-assisted capillary compression method, Huang's group fabricated a paper-ball-like 3D graphene structure that was composed of crumpled rGO sheets.[177] To prepare it, a GO aqueous solution was first sprayed into a tube furnace heated at 800 °C with the carrying gas of N_2 (Fig. 5e). During the rapid evaporation of the solvent of GO droplets, GO sheets were compressed and aggregated to form the 3D graphene structure with a morphology similar to that of crumpled paper balls (Fig. 5f). In this process, the GO was simultaneously thermally reduced to rGO. Importantly, the GSs showed high compressive strength, which gave them an interesting aggregation-resistant property. As we know, flat graphene sheets are easily stacked to form a graphitic structure, which makes dispersion of dried graphene materials extremely difficult. However, even after the GSs were compressed at a high pressure of 2 GPa, they could still be redispersed in a solvent. Moreover, various GS-based composites, *e.g.* the crumpled graphene (CG) spheres composited with SnO_2 or Mn_3O_4 (Fig. 5g and h), have also been obtained by spraying the metals, metal oxides or their precursors together with the GO dispersion into a furnace, which extends the applications of GSs in supercapacitors and lithium-ion batteries.[39,175]

3.6. Other types of 3D graphene structures

In addition to the aforementioned 3D structures, other types of graphene structures, such as onion rings,[182] honeycombs,[183,184] scrolls,[185–191] nanosacks,[192,193] and erythrocyte-like microspheres,[194] have also been reported, which exhibited their unique properties and applications.

For example, Tour *et al.* synthesized hexagonal graphene onion rings by a CVD method.[182] In this unique structure, a number of graphene nanoribbons were grown beneath a monolayer graphene sheet, and formed a nearly concentric onion ring-like structure (Fig. 6a and b). Importantly, after removing the top monolayer graphene sheet by argon plasma, graphene nanoribbons, a promising graphene material with a width-dependent band gap for electronics,[195] can be obtained. The resultant graphene nanoribbons exhibited high binding energy for lithium ions, and therefore have potential usage in lithium ion storage.

Honeycomb-like 3D graphene structures are mostly prepared by self-assembly of GO sheets,[184,196,197] which have been used in the applications of supercapacitors[197,198] and dye-sensitized solar cells (DSSC).[183] As an interesting example, Li *et al.* used a freeze-casting method to fabricate a 3D graphene with a honeycomb-like structure, where ice crystals played the role of template.[184] The obtained honeycomb-like 3D graphene exhibited excellent mechanical strength and elasticity, which could sustain a compression strain of 80% and fully recover its original shape and size. This 3D graphene material also showed

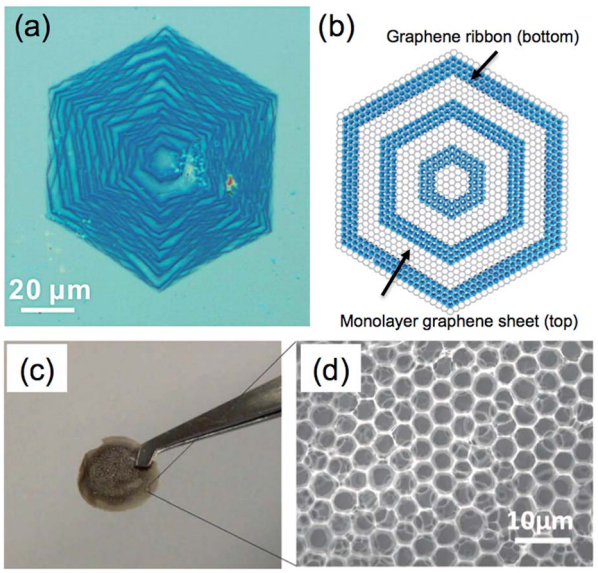

Fig. 6 (a) Optical image and (b) structural model of hexagonal graphene onion rings (HGoRs). Reproduced with permission from ref. 182. Copyright 2013, American Chemical Society. (c) Photograph and (d) SEM image of a freestanding 3D honeycomb-like graphene film. Reproduced with permission from ref. 196. Copyright 2013, WILEY-VCH Verlag GmbH & Co. KGaA.

a high porosity of ~99.98% with a density as low as ~0.5 mg cm^{-3}. In addition, Chen *et al.* fabricated a freestanding 3D honeycomb-like graphene film using a complex of dimethyldioctadecylammonium (DODA) and GO sheets (Fig. 6c and d).[196] Recently, a honeycomb-like 3D graphene structure was also obtained from the reaction between Li_2O powder and CO gas at 550 °C under low pressure for 12–24 h.[183] The counter electrode made of this 3D graphene exhibited an energy conversion efficiency of up to 7.8% in a DSSC, which is comparable to that using a Pt electrode (8%).

Carbon nanoscrolls, a novel 3D graphene structure prepared by wrapping graphene sheets into a tubular shape, has been revealed as promising in energy storage[186,188] and electronic devices.[185,191] Recently, our group developed a scalable method to produce well-aligned GO scrolls on various substrates.[185] After the reduction process, the resultant rGO scrolls were used as a gas sensor, which exhibited a detection limit of 0.4 ppm towards NO_2 gas.

4. Supercapacitor application

Supercapacitors, promising electrochemical energy storage devices with the advantages of high power density and long cycle life, have been attracting researchers' increasing interests due to their potential applications ranging from portable electronics to electric vehicles.[199–202] Based on the different charge storage mechanisms, supercapacitors can be divided into electric double-layer capacitors (EDLCs) and pesudocapacitors. The charge storage mechanism of EDLCs relies on the separation of charges at the interface of the electrolyte and electrode, while pesudocapacitors are operated following the mechanism of reversible redox reactions occurring at the surface or near-surface areas of active materials.[199] Carbonaceous materials, such as activated carbons, carbon nanotubes and graphene, have been widely employed for the construction of supercapacitor electrodes, due to their low cost, electrical conductivity and high surface area.[203–211] Recently, 3D graphene-based materials have been proven as promising candidates for supercapacitors.[40,155] The unique properties and porous structures of 3DGMs not only improve the accessibility of electrolyte to the surface of the electrode, but also provide electrically conductive channels for the active materials decorated on them, which enhance the performances of both EDLCs and pesudocapacitors. In this section, the supercapacitor applications of different types of 3D graphene structures and their composites are summarized. The flexible supercapacitor, especially the fiber-based supercapacitor, is also reviewed.

3DGMs with various structures, such as hydrogels,[111,112] aerogels,[94,212] sponges[110] and porous films,[149,154,155] have been extensively explored in the application of supercapacitors. As a typical example, a 3D porous graphene with extremely high surface area of 3100 $m^2 g^{-1}$, produced by chemical activation of microwave exfoliated graphene oxides (MEGO), was used for constructing a symmetrical supercapacitor with ionic liquid and organic electrolytes.[155] The activated MEGO (a-MEGO) contained numerous small pores with sizes ranging from ~1 to 10 nm, and also possessed a high electrical conductivity of ~500 S m^{-1}. The supercapacitor delivered a specific capacitance of 150 F g^{-1} at a current density of 0.8 A g^{-1} with a small equivalent series resistance (ESR) of 4.6 ohms. Moreover, their subsequent work further demonstrated that the a-MEGO-based supercapacitor was capable of operation below room temperature (down to −50 °C), giving a specific capacitance over 100 F g^{-1}.[213] Although more effective surface area of graphene can be obtained by construction of 3D graphene structures, the specific capacitances in previously reported graphene electrodes are still far from the theoretical capacitance of graphene, *e.g.* 550 F g^{-1} calculated based on the intrinsic capacitance and theoretical specific surface area of graphene.[214,215]

3D porous graphene films composited with pseudo-capacitive materials that have high theoretical capacitances, such as metal oxides and conducting redox polymers, have been widely explored for improving the supercapacitor performance of 3DGMs.[216–218] Higher specific capacitance and energy density, better rate capability and longer cycling life have been observed in the composite electrodes.[112,212] For example, the $Ni(OH)_2$/graphene composite prepared by Dai *et al.* exhibited a specific capacitance of ~877 F g^{-1} at 40 mV s^{-1}, while only 339 F g^{-1} for the physical mixture of these two components was obtained.[219] Even at a high current density of 45.7 A g^{-1}, a specific capacitance of ~953 F g^{-1} was still retained for the $Ni(OH)_2$/graphene composite. After a cycling test at 28.6 A g^{-1} for 2000 cycles, the electrode of $Ni(OH)_2$/graphene composite showed a negligible change of capacitance. The enhanced supercapacitor performance of composites is generally attributed to the synergetic effect of graphene and the other components.[216] First, the pseudo-capacitive materials not only contribute pseudo-capacitance to the whole composite electrode, but also act as spacer

materials to enlarge the interspace between graphene sheets, resulting in the improved accessibility of electrolyte to the electrode. Second, the interconnected graphene sheets provide electrically conductive channels to the composite, which enables fast charge transport in the composite and preserves the good performance of electrode at a high charge–discharge current density.

Graphene spheres (GS) have a relatively stable structure with high surface area in aqueous solvent.[88,177] Since GS can be prepared by scalable methods, it makes GS suitable for the construction of supercapacitor electrodes.[39,44,180] For example, mesoporous graphene nanoballs (MGBs) are able to be obtained on the gram scale by a CVD method, which showed a high surface area of 508 $m^2 g^{-1}$ and conductivity of 1.7 S cm^{-1}.[44] After a subsequent doping process to increase the conductivity of MGB to 6.5 S cm^{-1}, the p-doped MGB exhibited a specific capacitance of 206 F g^{-1} at 5 mV s^{-1} and over 96% retention of the initial capacitance after 10 000 cycles at a relatively high current density of 20 A g^{-1} in an electrolyte of 1 mol L^{-1} H_2SO_4. The excellent performance of p-doped MGB is attributed to the high conductivity of the CVD-produced graphene, and its mesoporous structure with a mean pore size of 4.27 nm, which enables the electrolyte to easily access the inner surface of the MGB. The performance of GS-based supercapacitors has been improved further by the combination of GS with pseudocapacitive materials.[39] Chen *et al.* reported the direct deposition of graphene–Mn_3O_4 composite spheres on indium tin oxide (ITO) substrate by an aerosolization method. The obtained electrode exhibited a specific capacitance of 1027 F g^{-1} at a current density of 5 A g^{-1} and 404 F g^{-1} at a high current density of 40 A g^{-1}. After testing for 1000 cycles at a current density of 20 A g^{-1}, the GS-based composite electrode still retained 78% capacitance.[39]

Direct coating of graphene on a 3D substrate followed by the functionalization of graphene with other pseudo-capacitive materials is a convenient and effective way to apply 3D graphene in supercapacitors.[91,94,105] For instance, Bao *et al.* developed a MnO_2/graphene/textile composite electrode by using the template of 3D porous textile fibers.[105] This composite electrode was fabricated through coating textile fibers with solution-exfoliated graphene sheets, followed by electrodeposition of pseudocapacitive MnO_2 NPs onto the surface of the graphene/textile fibers. The coated graphene layer not only increased the electrical conductivity of the fabricated electrodes, but also improved the adhesion of the textile fibers to the active materials. The composite electrode showed a specific capacitance of ~315 F g^{-1} at a scan rate of 2 mV s^{-1}. An asymmetrical supercapacitor operated in 0.5 mol L^{-1} Na_2SO_4 aqueous electrolyte was also fabricated by using the MnO_2/graphene/textile and CNT/textile as the positive and negative electrode, respectively. This asymmetrical supercapacitor delivered a power density of 110 kW kg^{-1} and an energy density of 12.5 W h kg^{-1}, and also exhibited excellent cycling performance with ~95% retention of the initial specific capacitance after 5000 cycles.

Recently, 3DGNs,[37] prepared by a CVD method based on the template of Ni foam, have been demonstrated as a promising material for the fabrication of supercapacitor electrodes.[40] To date, a number of materials have been composited with 3DGNs, and some of the 3DGN-based composites have shown excellent supercapacitor performances.[118,119,123,220,221] For example, our group used a simple electrochemical deposition method to fabricate a NiO/3DGN composite electrode for supercapacitor, which produced a specific capacitance of 745 F g^{-1} at a current density of 1.4 A g^{-1}.[40] The excellent electrical contacts among the active material of NiO, graphene sheets and the current collector of Ni foam allowed rapid charge transfer within this composite. Meanwhile, the porous structure of 3DGNs facilitated the easy accessibility of electrolyte ions to the active materials. An asymmetric supercapacitor was also fabricated by using $Ni(OH)_2$/3DGN and a-MEGO as the positive and negative electrodes, respectively.[221] The obtained supercapacitor showed a high power density of 44.0 kW kg^{-1} in the aqueous electrolyte of 6 mol L^{-1} KOH, which is much higher than that of commercially available supercapacitors. Moreover, a hierarchical nanostructure, which was composed of 3DGNs coated with two different components, has been successfully prepared by our group and used as a supercapacitor electrode. In the aforementioned work, the Ni_3S_2@$Ni(OH)_2$/3DGN was obtained through a one-step hydrothermal reaction, in which the crystalline Ni_3S_2 nanorods coated with $Ni(OH)_2$ nanosheets were grown on the surface of 3DGNs (Fig. 7a).[119] The highly crystalline Ni_3S_2 nanorods that grew perpendicularly to the surface of 3DGNs played an essential role in the supercapacitor performance of the Ni_3S_2@$Ni(OH)_2$/3DGN composite, which not only served as electrically conductive channels to improve the electron transport performance of coated $Ni(OH)_2$ sheets, but also increased the contact area of $Ni(OH)_2$ with electrolyte. Due to the unique hierarchical nanostructure, the supercapacitor performance of Ni_3S_2@$Ni(OH)_2$/3DGN was much better than those of both Ni_3S_2/3DGN and $Ni(OH)_2$/3DGN, which exhibited high specific capacitances of 1277 F g^{-1} at 2 mV s^{-1} and 1037.5 F g^{-1} at 5.1 A g^{-1}, and also high areal capacitances of 4.7 F cm^{-2} at 2 mV s^{-1} and 3.85 F cm^{-2} at 19.1 mA cm^{-2}. The obtained Ni_3S_2@$Ni(OH)_2$/3DGN also showed an excellent cycling performance, as it was able to retain 99.1% of the initial specific capacitance even after 2000-cycle operation.

Flexible supercapacitors are of great importance, because they are the potential power supplies for next-generation wearable devices, *e.g.* electronic textiles.[222] Due to their excellent mechanical and electrical properties, 3D graphene architectures, especially graphene fibers,[43,143,170,223] porous films,[45,152] and networks,[220,224] have played essential roles in the fabrication of flexible supercapacitor devices. For example, Xie *et al.* fabricated a flexible and lightweight symmetrical supercapacitor based on the MnO_2/3DGN composite.[220] Before the growth of 3DGNs by CVD, the Ni foam template was first pressed to form a more compact 3D structure, which reduced the pore size and increased the volume density of the synthesized 3DGNs. Importantly, this process also improved the flexibility of the 3DGNs. The resultant 3DGN electrodes showed negligible resistance variations under bending with the angle up to 180° (Fig. 7b). After electrodeposition of MnO_2 nanospheres on the 3DGNs, the obtained MnO_2/3DGN composite showed a large specific surface area (392 $m^2 g^{-1}$) and an extremely high mass

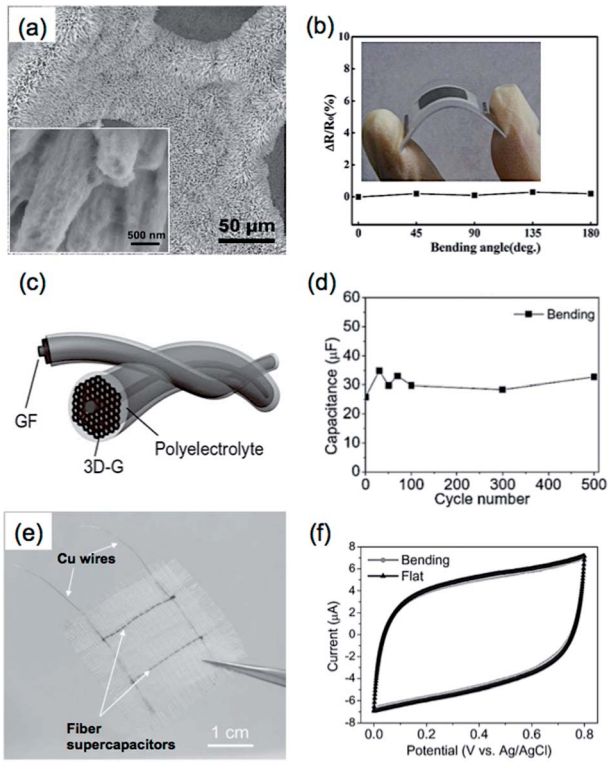

Fig. 7 (a) SEM image of Ni_3S_2@$Ni(OH)_2$/3DGN composite. Inset: high-magnification SEM image of the Ni_3S_2@$Ni(OH)_2$ coated on 3DGN. Reproduced from ref. 119 with permission from The Royal Society of Chemistry. (b) Resistance changes ($\Delta R/R$) of 3DGN electrodes at different bending angles. Inset: photograph of a flexible MnO_2/3DGN composite supercapacitor. Reproduced with permission from ref. 220. Copyright 2013, American Chemical Society. (c) Schematic illustration of the configuration of an all-solid-state GF supercapacitor. (d) Cyclability of a GF supercapacitor after bending for 500 cycles. (e) Photograph of a flexible supercapacitor device fabricated by integrating two GF supercapacitors into a textile. (f) Cyclic voltammetry (CV) curves of the flexible supercapacitor device in (e) the flat and bending states at a scan rate of 50 mV s^{-1}. Reproduced with permission from ref. 43. Copyright 2013, WILEY-VCH Verlag GmbH & Co. KGaA.

loading of 92.9% MnO_2. The symmetrical supercapacitor based on the MnO_2/3DGN composite delivered an areal capacitance of 1.42 F cm^{-2} and a specific capacitance of 130 F g^{-1} at a scan rate of 2 mV s^{-1}.

Fiber-based supercapacitors (FSs) are promising candidates for flexible energy storage devices.[225,226] Many fiber materials including ZnO[227] and CNTs[228,229] have been developed and investigated in this area. FSs were prepared by coating graphene on fiber materials to enhance the supercapacitor performance.[230–233] However, the flexibility and performance of those reported FSs still require further improvement.

Graphene fibers (GF) have the advantages of flexibility, conductivity, large surface area and easy functionalization, giving them great potential for the construction of FS.[234] As a typical example, Qu *et al.* fabricated an all-solid-state GF supercapacitor, in which two GFs were intertwisted together with H_2SO_4–polyvinyl alcohol (PVA) gel as electrolyte (Fig. 7c).[43] The fabricated GF-based supercapacitors exhibited an areal capacitance of 1.2–1.7 mF cm^{-2}, and a stable electrochemical performance without an obvious change in capacitance after bending for 500 cycles (Fig. 7d). Interestingly, a flexible supercapacitor device was fabricated by weaving two GF-based supercapacitors into a textile, which showed negligible variation in the cyclic voltammetry (CV) curves before and after bending (Fig. 7e and f). The functionalization of GFs with active materials is able to improve the energy density of a GF-based supercapacitor.[170,235] In a recent work, Zhu *et al.* prepared a MnO_2-coated GF based on the high electrically conductive CVD-grown graphene film, which exhibited an areal capacitance of 42 mF cm^{-2} at 10 mV s^{-1} with an energy density of 1.46×10^{-3} mW h cm^{-2}.[235]

5. Conclusions

3D graphene materials (3DGMs) have been proven as promising in a wide area of research interests. Up to now, a number of 3DGMs with different structures and varied functions have been reported. These novel materials not only preserve the intrinsic properties of the individual 2D graphene sheet, but also provide a tremendous opportunity to explore graphene in various practical applications. For example, graphene with a porous 3D macroscopic structure, having high electrical conductivity, large surface area and high mechanical strength, can be used directly or after decoration with electroactive materials as a supercapacitor electrode.

Although lots of strategies on the construction of 3DGMs with specific morphologies have been demonstrated, there are still some challenges. The properties of 3DGMs are related to their structure, but the precise control of pore size and porosity of 3DGMs has not been achieved. Most of the reported 3DGMs showed a wide pore size distribution ranging from a few hundred nanometers to several hundred micrometers. The fabrication of 3D graphene architectures with uniform meso- or micro-pores is still a challenge. There are also few reports on the preparation of freestanding and macroscopic 3DGMs that are composed of a single-layer graphene film, mostly due to its insufficient mechanical strength. To address these issues, it could be feasible to choose nanoporous graphene sheets including graphene nanomeshes[84,236,237] and mesoporous graphene sheets[155,238,239] with uniform pore sizes in the graphene, as building blocks, which are then assembled into 3D macroscopic structures. Of course, more efforts and experiments are required to obtain a more controllable and efficient method for the fabrication of 3DGMs for practical applications.

Recently, graphene-like 2D nanosheets, such as transition metal dichalcogenides,[240–248] have been attracting increasing attention. The future direction will be to assemble these novel 2D materials into 3D macroscopic structures, and investigate their unique properties and various applications.

Acknowledgements

This work was supported by MOE under AcRF Tier 2 (ARC 26/13, No. MOE2013-T2-1-034), AcRF Tier 1 (RG 61/12, RGT18/13), and Start-Up Grant (M4080865.070.706022) in Singapore. This

research is also conducted by NTU-HUJ-BGU Nanomaterials for Energy and Water Management Programme under the Campus for Research Excellence and Technological Enterprise (CREATE), that is supported by the National Research Foundation, Prime Minister's Office, Singapore.

Notes and references

1 K. S. Novoselov, A. K. Geim, S. V. Morozov, D. Jiang, Y. Zhang, S. V. Dubonos, I. V. Grigorieva and A. A. Firsov, *Science*, 2004, **306**, 666–669.
2 M. J. Allen, V. C. Tung and R. B. Kaner, *Chem. Rev.*, 2010, **110**, 132–145.
3 X. Huang, X. Qi, F. Boey and H. Zhang, *Chem. Soc. Rev.*, 2012, **41**, 666–686.
4 X. Huang, Z. Yin, S. Wu, X. Qi, Q. He, Q. Zhang, Q. Yan, F. Boey and H. Zhang, *Small*, 2011, **7**, 1876–1902.
5 A. A. Balandin, S. Ghosh, W. Bao, I. Calizo, D. Teweldebrhan, F. Miao and C. N. Lau, *Nano Lett.*, 2008, **8**, 902–907.
6 S. Stankovich, D. A. Dikin, G. H. B. Dommett, K. M. Kohlhaas, E. J. Zimney, E. A. Stach, R. D. Piner, S. T. Nguyen and R. S. Ruoff, *Nature*, 2006, **442**, 282–286.
7 R. R. Nair, P. Blake, A. N. Grigorenko, K. S. Novoselov, T. J. Booth, T. Stauber, N. M. R. Peres and A. K. Geim, *Science*, 2008, **320**, 1308.
8 C. Lee, X. Wei, J. W. Kysar and J. Hone, *Science*, 2008, **321**, 385–388.
9 P. W. Sutter, J.-I. Flege and E. A. Sutter, *Nat. Mater.*, 2008, **7**, 406–411.
10 K. V. Emtsev, A. Bostwick, K. Horn, J. Jobst, G. L. Kellogg, L. Ley, J. L. McChesney, T. Ohta, S. A. Reshanov, J. Rohrl, E. Rotenberg, A. K. Schmid, D. Waldmann, H. B. Weber and T. Seyller, *Nat. Mater.*, 2009, **8**, 203–207.
11 D. Li, M. B. Muller, S. Gilje, R. B. Kaner and G. G. Wallace, *Nat. Nanotechnol.*, 2008, **3**, 101–105.
12 K. S. Kim, Y. Zhao, H. Jang, S. Y. Lee, J. M. Kim, K. S. Kim, J.-H. Ahn, P. Kim, J.-Y. Choi and B. H. Hong, *Nature*, 2009, **457**, 706–710.
13 X. Li, W. Cai, J. An, S. Kim, J. Nah, D. Yang, R. Piner, A. Velamakanni, I. Jung, E. Tutuc, S. K. Banerjee, L. Colombo and R. S. Ruoff, *Science*, 2009, **324**, 1312–1314.
14 Q. He, S. Wu, S. Gao, X. Cao, Z. Yin, H. Li, P. Chen and H. Zhang, *ACS Nano*, 2011, **5**, 5038–5044.
15 X. Huang, Z. Zeng, Z. Fan, J. Liu and H. Zhang, *Adv. Mater.*, 2012, **24**, 5979–6004.
16 B. Li, X. Cao, H. G. Ong, J. W. Cheah, X. Zhou, Z. Yin, H. Li, J. Wang, F. Boey, W. Huang and H. Zhang, *Adv. Mater.*, 2010, **22**, 3058–3061.
17 J. Liu, Z. Lin, T. Liu, Z. Yin, X. Zhou, S. Chen, L. Xie, F. Boey, H. Zhang and W. Huang, *Small*, 2010, **6**, 1536–1542.
18 J. Liu, Z. Yin, X. Cao, F. Zhao, A. Lin, L. Xie, Q. Fan, F. Boey, H. Zhang and W. Huang, *ACS Nano*, 2010, **4**, 3987–3992.
19 J. Liu, Z. Yin, X. Cao, F. Zhao, L. Wang, W. Huang and H. Zhang, *Adv. Mater.*, 2013, **25**, 233–238.
20 J. Liu, Z. Zeng, X. Cao, G. Lu, L.-H. Wang, Q.-L. Fan, W. Huang and H. Zhang, *Small*, 2012, **8**, 3517–3522.
21 X. Qi, C. Tan, J. Wei and H. Zhang, *Nanoscale*, 2013, **5**, 1440–1451.
22 Z. Yin, Z. Zeng, J. Liu, Q. He, P. Chen and H. Zhang, *Small*, 2013, **9**, 727–731.
23 Z. Yin, J. Zhu, Q. He, X. Cao, C. Tan, H. Chen, Q. Yan and H. Zhang, *Adv. Energy Mater.*, 2014, **4**, 1300574.
24 J. Zhu, D. Yang, Z. Yin, Q. Yan and H. Zhang, *Small*, 2014, DOI: 10.1002/smll.201303202.
25 M. He, J. Jung, F. Qiu and Z. Lin, *J. Mater. Chem.*, 2012, **22**, 24254–24264.
26 J. Song, Z. Yin, Z. Yang, P. Amaladass, S. Wu, J. Ye, Y. Zhao, W.-Q. Deng, H. Zhang and X.-W. Liu, *Chem.–Eur. J.*, 2011, **17**, 10832–10837.
27 Z. Yin, S. Sun, T. Salim, S. Wu, X. Huang, Q. He, Y. M. Lam and H. Zhang, *ACS Nano*, 2010, **4**, 5263–5268.
28 Z. Yin, S. Wu, X. Zhou, X. Huang, Q. Zhang, F. Boey and H. Zhang, *Small*, 2010, **6**, 307–312.
29 Q. He, S. Wu, Z. Yin and H. Zhang, *Chem. Sci.*, 2012, **3**, 1764–1772.
30 S. Wu, Q. He, C. Tan, Y. Wang and H. Zhang, *Small*, 2013, **9**, 1160–1172.
31 Y. Shao, J. Wang, H. Wu, J. Liu, I. A. Aksay and Y. Lin, *Electroanalysis*, 2010, **22**, 1027–1036.
32 Q. He, H. G. Sudibya, Z. Yin, S. Wu, H. Li, F. Boey, W. Huang, P. Chen and H. Zhang, *ACS Nano*, 2010, **4**, 3201–3208.
33 G. Lu, H. Li, C. Liusman, Z. Yin, S. Wu and H. Zhang, *Chem. Sci.*, 2011, **2**, 1817–1821.
34 H. G. Sudibya, Q. He, H. Zhang and P. Chen, *ACS Nano*, 2011, **5**, 1990–1994.
35 Z. Wang, J. Zhang, P. Chen, X. Zhou, Y. Yang, S. Wu, L. Niu, Y. Han, L. Wang, P. Chen, F. Boey, Q. Zhang, B. Liedberg and H. Zhang, *Biosens. Bioelectron.*, 2011, **26**, 3881–3886.
36 Z. Yin, Q. He, X. Huang, J. Zhang, S. Wu, P. Chen, G. Lu, P. Chen, Q. Zhang, Q. Yan and H. Zhang, *Nanoscale*, 2012, **4**, 293–297.
37 Z. Chen, W. Ren, L. Gao, B. Liu, S. Pei and H.-M. Cheng, *Nat. Mater.*, 2011, **10**, 424–428.
38 W. Li, S. Gao, L. Wu, S. Qiu, Y. Guo, X. Geng, M. Chen, S. Liao, C. Zhu, Y. Gong, M. Long, J. Xu, X. Wei, M. Sun and L. Liu, *Sci. Rep.*, 2013, **3**, 2125.
39 S. Mao, Z. Wen, H. Kim, G. Lu, P. Hurley and J. Chen, *ACS Nano*, 2012, **6**, 7505–7513.
40 X. Cao, Y. Shi, W. Shi, G. Lu, X. Huang, Q. Yan, Q. Zhang and H. Zhang, *Small*, 2011, **7**, 3163–3168.
41 H. S. Ahn, J. M. Kim, C. Park, J.-W. Jang, J. S. Lee, H. Kim, M. Kaviany and M. H. Kim, *Sci. Rep.*, 2013, **3**, 1960.
42 S. Mao, K. Yu, J. Chang, D. A. Steeber, L. E. Ocola and J. Chen, *Sci. Rep.*, 2013, **3**, 1696.
43 Y. N. Meng, Y. Zhao, C. G. Hu, H. H. Cheng, Y. Hu, Z. P. Zhang, G. Q. Shi and L. T. Qu, *Adv. Mater.*, 2013, **25**, 2326–2331.
44 J.-S. Lee, S.-I. Kim, J.-C. Yoon and J.-H. Jang, *ACS Nano*, 2013, **7**, 6047–6055.
45 Z. Niu, J. Chen, H. H. Hng, J. Ma and X. Chen, *Adv. Mater.*, 2012, **24**, 4144–4150.

46 D. R. Dreyer, S. Park, C. W. Bielawski and R. S. Ruoff, *Chem. Soc. Rev.*, 2010, **39**, 228–240.
47 X. Huang, S. Li, S. Wu, Y. Huang, F. Boey, C. L. Gan and H. Zhang, *Adv. Mater.*, 2012, **24**, 979–983.
48 X. Huang, X. Zhou, S. Wu, Y. Wei, X. Qi, J. Zhang, F. Boey and H. Zhang, *Small*, 2010, **6**, 513–516.
49 H. Li, X. Cao, B. Li, X. Zhou, G. Lu, C. Liusman, Q. He, F. Boey, S. S. Venkatraman and H. Zhang, *Chem. Commun.*, 2011, **47**, 10070–10072.
50 X. Qi, H. Li, J. W. Y. Lam, X. Yuan, J. Wei, B. Z. Tang and H. Zhang, *Adv. Mater.*, 2012, **24**, 4191–4195.
51 X. Qi, K.-Y. Pu, H. Li, X. Zhou, S. Wu, Q.-L. Fan, B. Liu, F. Boey, W. Huang and H. Zhang, *Angew. Chem., Int. Ed.*, 2010, **49**, 9426–9429.
52 X. Qi, K.-Y. Pu, X. Zhou, H. Li, B. Liu, F. Boey, W. Huang and H. Zhang, *Small*, 2010, **6**, 663–669.
53 Z. Wang, J. Zhang, Z. Yin, S. Wu, D. Mandler and H. Zhang, *Nanoscale*, 2012, **4**, 2728–2733.
54 S. Wu, Q. He, C. Zhou, X. Qi, X. Huang, Z. Yin, Y. Yang and H. Zhang, *Nanoscale*, 2012, **4**, 2478–2483.
55 S. Wu, Z. Yin, Q. He, G. Lu, Q. Yan and H. Zhang, *J. Phys. Chem. C*, 2011, **115**, 15973–15979.
56 S. Bae, H. Kim, Y. Lee, X. Xu, J.-S. Park, Y. Zheng, J. Balakrishnan, T. Lei, H. Ri Kim, Y. I. Song, Y.-J. Kim, K. S. Kim, B. Ozyilmaz, J.-H. Ahn, B. H. Hong and S. Iijima, *Nat. Nanotechnol.*, 2010, **5**, 574–578.
57 H. Bai, C. Li, X. Wang and G. Shi, *J. Phys. Chem. C*, 2011, **115**, 5545–5551.
58 H. Bai, C. Li, X. Wang and G. Shi, *Chem. Commun.*, 2010, **46**, 2376–2378.
59 O. C. Compton, Z. An, K. W. Putz, B. J. Hong, B. G. Hauser, L. Catherine Brinson and S. T. Nguyen, *Carbon*, 2012, **50**, 3399–3406.
60 Y. Xu, Q. Wu, Y. Sun, H. Bai and G. Shi, *ACS Nano*, 2010, **4**, 7358–7362.
61 H.-P. Cong, X.-C. Ren, P. Wang and S.-H. Yu, *ACS Nano*, 2012, **6**, 2693–2703.
62 Z.-S. Wu, S. Yang, Y. Sun, K. Parvez, X. Feng and K. Müllen, *J. Am. Chem. Soc.*, 2012, **134**, 9082–9085.
63 Y. Chang, J. Li, B. Wang, H. Luo, H. He, Q. Song and L. Zhi, *J. Mater. Chem. A*, 2013, **1**, 14658–14665.
64 S. Sun and P. Wu, *J. Mater. Chem.*, 2011, **21**, 4095–4097.
65 P. M. Sudeep, T. N. Narayanan, A. Ganesan, M. M. Shaijumon, H. Yang, S. Ozden, P. K. Patra, M. Pasquali, R. Vajtai, S. Ganguli, A. K. Roy, M. R. Anantharaman and P. M. Ajayan, *ACS Nano*, 2013, **7**, 7034–7040.
66 H. Sun, Z. Xu and C. Gao, *Adv. Mater.*, 2013, **25**, 2554–2560.
67 S. Korkut, J. D. Roy-Mayhew, D. M. Dabbs, D. L. Milius and I. A. Aksay, *ACS Nano*, 2011, **5**, 5214–5222.
68 X. Yang, J. Zhu, L. Qiu and D. Li, *Adv. Mater.*, 2011, **23**, 2833–2838.
69 F. Liu and T. S. Seo, *Adv. Funct. Mater.*, 2010, **20**, 1930–1936.
70 K. Sheng, Y. Sun, C. Li, W. Yuan and G. Shi, *Sci. Rep.*, 2012, **2**, 247.
71 M. A. Worsley, T. Y. Olson, J. R. I. Lee, T. M. Willey, M. H. Nielsen, S. K. Roberts, P. J. Pauzauskie, J. Biener, J. H. Satcher and T. F. Baumann, *J. Phys. Chem. Lett.*, 2011, **2**, 921–925.
72 M. A. Worsley, P. J. Pauzauskie, T. Y. Olson, J. Biener, J. H. Satcher and T. F. Baumann, *J. Am. Chem. Soc.*, 2010, **132**, 14067–14069.
73 Y. Xu, K. Sheng, C. Li and G. Shi, *ACS Nano*, 2010, **4**, 4324–4330.
74 Z. Tang, S. Shen, J. Zhuang and X. Wang, *Angew. Chem., Int. Ed.*, 2010, **49**, 4603–4607.
75 W. Wei, S. Yang, H. Zhou, I. Lieberwirth, X. Feng and K. Müllen, *Adv. Mater.*, 2013, **25**, 2909–2914.
76 X. Xie, Y. Zhou, H. Bi, K. Yin, S. Wan and L. Sun, *Sci. Rep.*, 2013, **3**, 2117.
77 Y. Su, Y. Zhang, X. Zhuang, S. Li, D. Wu, F. Zhang and X. Feng, *Carbon*, 2013, **62**, 296–301.
78 Z. Han, Z. Tang, P. Li, G. Yang, Q. Zheng and J. Yang, *Nanoscale*, 2013, **5**, 5462–5467.
79 H. Bi, X. Xie, K. Yin, Y. Zhou, S. Wan, L. He, F. Xu, F. Banhart, L. Sun and R. S. Ruoff, *Adv. Funct. Mater.*, 2012, **22**, 4421–4425.
80 Y. Tao, X. Xie, W. Lv, D.-M. Tang, D. Kong, Z. Huang, H. Nishihara, T. Ishii, B. Li, D. Golberg, F. Kang, T. Kyotani and Q.-H. Yang, *Sci. Rep.*, 2013, **3**, 2975.
81 W. Chen, S. Li, C. Chen and L. Yan, *Adv. Mater.*, 2011, **23**, 5679–5683.
82 Z. Chen, W. Ren, B. Liu, L. Gao, S. Pei, Z.-S. Wu, J. Zhao and H.-M. Cheng, *Carbon*, 2010, **48**, 3543–3550.
83 M. Zhou, T. Lin, F. Huang, Y. Zhong, Z. Wang, Y. Tang, H. Bi, D. Wan and J. Lin, *Adv. Funct. Mater.*, 2013, **23**, 2263–2269.
84 G. Ning, Z. Fan, G. Wang, J. Gao, W. Qian and F. Wei, *Chem. Commun.*, 2011, **47**, 5976–5978.
85 X. Xiao, T. E. Beechem, M. T. Brumbach, T. N. Lambert, D. J. Davis, J. R. Michael, C. M. Washburn, J. Wang, S. M. Brozik, D. R. Wheeler, D. B. Burckel and R. Polsky, *ACS Nano*, 2012, **6**, 3573–3579.
86 X. Xiao, J. R. Michael, T. Beechem, A. McDonald, M. Rodriguez, M. T. Brumbach, T. N. Lambert, C. M. Washburn, J. Wang, S. M. Brozik, D. R. Wheeler, D. B. Burckel and R. Polsky, *J. Mater. Chem.*, 2012, **22**, 23749–23754.
87 R. Wang, Y. Hao, Z. Wang, H. Gong and J. T. L. Thong, *Nano Lett.*, 2010, **10**, 4844–4850.
88 S.-M. Yoon, W. M. Choi, H. Baik, H.-J. Shin, I. Song, M.-S. Kwon, J. J. Bae, H. Kim, Y. H. Lee and J.-Y. Choi, *ACS Nano*, 2012, **6**, 6803–6811.
89 J.-S. Lee, H.-J. Ahn, J.-C. Yoon and J.-H. Jang, *Phys. Chem. Chem. Phys.*, 2012, **14**, 7938–7943.
90 X. H. Xia, J. P. Tu, Y. J. Mai, R. Chen, X. L. Wang, C. D. Gu and X. B. Zhao, *Chem.–Eur. J.*, 2011, **17**, 10898–10905.
91 J. Chen, K. Sheng, P. Luo, C. Li and G. Shi, *Adv. Mater.*, 2012, **24**, 4569–4573.
92 H. Wang, G. Wang, Y. Ling, F. Qian, Y. Song, X. Lu, S. Chen, Y. Tong and Y. Li, *Nanoscale*, 2013, **5**, 10283–10290.
93 T. Zhai, F. Wang, M. Yu, S. Xie, C. Liang, C. Li, F. Xiao, R. Tang, Q. Wu, X. Lu and Y. Tong, *Nanoscale*, 2013, **5**, 6790–6796.

94 S. Ye, J. Feng and P. Wu, *ACS Appl. Mater. Interfaces*, 2013, **5**, 7122–7129.
95 J.-C. Yoon, J.-S. Lee, S.-I. Kim, K.-H. Kim and J.-H. Jang, *Sci. Rep.*, 2013, **3**, 1788.
96 X. Huang, K. Qian, J. Yang, J. Zhang, L. Li, C. Yu and D. Zhao, *Adv. Mater.*, 2012, **24**, 4419–4423.
97 G.-h. Moon, Y. Shin, D. Choi, B. W. Arey, G. J. Exarhos, C. Wang, W. Choi and J. Liu, *Nanoscale*, 2013, **5**, 6291–6296.
98 K. Sohn, Y. Joo Na, H. Chang, K.-M. Roh, H. Dong Jang and J. Huang, *Chem. Commun.*, 2012, **48**, 5968–5970.
99 H. Wang, D. Zhang, T. Yan, X. Wen, J. Zhang, L. Shi and Q. Zhong, *J. Mater. Chem. A*, 2013, **1**, 11778–11789.
100 B. G. Choi, M. Yang, W. H. Hong, J. W. Choi and Y. S. Huh, *ACS Nano*, 2012, **6**, 4020–4028.
101 L. Estevez, A. Kelarakis, Q. Gong, E. H. Da'as and E. P. Giannelis, *J. Am. Chem. Soc.*, 2011, **133**, 6122–6125.
102 H.-B. Yao, J. Ge, C.-F. Wang, X. Wang, W. Hu, Z.-J. Zheng, Y. Ni and S.-H. Yu, *Adv. Mater.*, 2013, **25**, 6692–6698.
103 D. D. Nguyen, N.-H. Tai, S.-B. Lee and W.-S. Kuo, *Energy Environ. Sci.*, 2012, **5**, 7908–7912.
104 W. Ouyang, J. Sun, J. Memon, C. Wang, J. Geng and Y. Huang, *Carbon*, 2013, **62**, 501–509.
105 G. Yu, L. Hu, M. Vosgueritchian, H. Wang, X. Xie, J. R. McDonough, X. Cui, Y. Cui and Z. Bao, *Nano Lett.*, 2011, **11**, 2905–2911.
106 Z. Bo, K. Yu, G. Lu, P. Wang, S. Mao and J. Chen, *Carbon*, 2011, **49**, 1849–1858.
107 K. Yu, P. Wang, G. Lu, K.-H. Chen, Z. Bo and J. Chen, *J. Phys. Chem. Lett.*, 2011, **2**, 537–542.
108 C. S. Rout, A. Kumar, T. S. Fisher, U. K. Gautam, Y. Bando and D. Golberg, *RSC Adv.*, 2012, **2**, 8250–8253.
109 C. Hu, X. Zhai, L. Liu, Y. Zhao, L. Jiang and L. Qu, *Sci. Rep.*, 2013, **3**, 2065.
110 Z. Xu, Z. Li, C. M. B. Holt, X. Tan, H. Wang, B. S. Amirkhiz, T. Stephenson and D. Mitlin, *J. Phys. Chem. Lett.*, 2012, **3**, 2928–2933.
111 P. Chen, J.-J. Yang, S.-S. Li, Z. Wang, T.-Y. Xiao, Y.-H. Qian and S.-H. Yu, *Nano Energy*, 2013, **2**, 249–256.
112 H. Gao, F. Xiao, C. B. Ching and H. Duan, *ACS Appl. Mater. Interfaces*, 2012, **4**, 2801–2810.
113 K. Chen, L. Chen, Y. Chen, H. Bai and L. Li, *J. Mater. Chem.*, 2012, **22**, 20968–20976.
114 M. S. Dresselhaus, A. Jorio, M. Hofmann, G. Dresselhaus and R. Saito, *Nano Lett.*, 2010, **10**, 751–758.
115 N. Li, Z. Chen, W. Ren, F. Li and H.-M. Cheng, *Proc. Natl. Acad. Sci. U. S. A.*, 2012, **109**, 17360–17365.
116 Z. Chen, C. Xu, C. Ma, W. Ren and H.-M. Cheng, *Adv. Mater.*, 2013, **25**, 1296–1300.
117 M. T. Pettes, H. Ji, R. S. Ruoff and L. Shi, *Nano Lett.*, 2012, **12**, 2959–2964.
118 X.-C. Dong, H. Xu, X.-W. Wang, Y.-X. Huang, M. B. Chan-Park, H. Zhang, L.-H. Wang, W. Huang and P. Chen, *ACS Nano*, 2012, **6**, 3206–3213.
119 W. Zhou, X. Cao, Z. Zeng, W. Shi, Y. Zhu, Q. Yan, H. Liu, J. Wang and H. Zhang, *Energy Environ. Sci.*, 2013, **6**, 2216–2221.
120 X. Cao, Z. Zeng, W. Shi, P. Yep, Q. Yan and H. Zhang, *Small*, 2012, **9**, 1703–1707.
121 X. Cao, Y. Shi, W. Shi, X. Rui, Q. Yan, J. Kong and H. Zhang, *Small*, 2013, 3433–3438.
122 Z. Yan, L. Ma, Y. Zhu, I. Lahiri, M. G. Hahm, Z. Liu, S. Yang, C. Xiang, W. Lu, Z. Peng, Z. Sun, C. Kittrell, J. Lou, W. Choi, P. M. Ajayan and J. M. Tour, *ACS Nano*, 2012, **7**, 58–64.
123 W. Wang, S. Guo, M. Penchev, I. Ruiz, K. N. Bozhilov, D. Yan, M. Ozkan and C. S. Ozkan, *Nano Energy*, 2013, **2**, 294–303.
124 F. Yavari, Z. Chen, A. V. Thomas, W. Ren, H.-M. Cheng and N. Koratkar, *Sci. Rep.*, 2011, **1**, 166.
125 H. Ji, L. Zhang, M. T. Pettes, H. Li, S. Chen, L. Shi, R. Piner and R. S. Ruoff, *Nano Lett.*, 2012, **12**, 2446–2451.
126 X. Cao, B. Zheng, X. Rui, W. Shi, Q. Yan and H. Zhang, *Angew. Chem., Int. Ed.*, 2014, **53**, 1404–1409.
127 J. Luo, J. Liu, Z. Zeng, C. F. Ng, L. Ma, H. Zhang, J. Lin, Z. Shen and H. J. Fan, *Nano Lett.*, 2013, **13**, 6136–6143.
128 Y.-H. Chang, C.-T. Lin, T.-Y. Chen, C.-L. Hsu, Y.-H. Lee, W. Zhang, K.-H. Wei and L.-J. Li, *Adv. Mater.*, 2013, **25**, 756–760.
129 Y. Xue, D. Yu, L. Dai, R. Wang, D. Li, A. Roy, F. Lu, H. Chen, Y. Liu and J. Qu, *Phys. Chem. Chem. Phys.*, 2013, **15**, 12220–12226.
130 B.-J. Kim, G. Yang, M. Joo Park, J. Seop Kwak, K. Hyeon Baik, D. Kim and J. Kim, *Appl. Phys. Lett.*, 2013, **102**, 161902–161904.
131 B. Tang, G. Hu, H. Gao and Z. Shi, *J. Power Sources*, 2013, **234**, 60–68.
132 N. Li, Q. Zhang, S. Gao, Q. Song, R. Huang, L. Wang, L. Liu, J. Dai, M. Tang and G. Cheng, *Sci. Rep.*, 2013, **3**, 1604.
133 C. Shan, H. Tang, T. Wong, L. He and S.-T. Lee, *Adv. Mater.*, 2012, **24**, 2491–2495.
134 Z. Sun, Z. Yan, J. Yao, E. Beitler, Y. Zhu and J. M. Tour, *Nature*, 2010, **468**, 549–552.
135 V. Sridhar, I. Lee, H.-S. Yoon, H.-H. Chun and H. Park, *Carbon*, 2013, **61**, 633–639.
136 Y. Li, Z. Li and P. K. Shen, *Adv. Mater.*, 2013, **25**, 2474–2480.
137 X. Wang, Y. Zhang, C. Zhi, X. Wang, D. Tang, Y. Xu, Q. Weng, X. Jiang, M. Mitome, D. Golberg and Y. Bando, *Nat. Commun.*, 2013, **4**, 2905.
138 Z. Fan, J. Yan, L. Zhi, Q. Zhang, T. Wei, J. Feng, M. Zhang, W. Qian and F. Wei, *Adv. Mater.*, 2010, **22**, 3723–3728.
139 D. Yu and L. Dai, *J. Phys. Chem. Lett.*, 2009, **1**, 467–470.
140 R. Jalili, S. H. Aboutalebi, D. Esrafilzadeh, K. Konstantinov, S. E. Moulton, J. M. Razal and G. G. Wallace, *ACS Nano*, 2013, **7**, 3981–3990.
141 Z. Lei, N. Christov and X. S. Zhao, *Energy Environ. Sci.*, 2011, **4**, 1866–1873.
142 Y. Sun, Q. Wu, Y. Xu, H. Bai, C. Li and G. Shi, *J. Mater. Chem.*, 2011, **21**, 7154–7160.
143 Q. Wu, Y. X. Xu, Z. Y. Yao, A. R. Liu and G. Q. Shi, *ACS Nano*, 2010, **4**, 1963–1970.
144 C. Liu, K. Wang, S. Luo, Y. Tang and L. Chen, *Small*, 2011, **7**, 1203–1206.
145 C. Tan, X. Huang and H. Zhang, *Mater. Today*, 2013, **16**, 29–36.

146 W. Shi, J. Zhu, D. H. Sim, Y. Y. Tay, Z. Lu, X. Zhang, Y. Sharma, M. Srinivasan, H. Zhang, H. H. Hng and Q. Yan, *J. Mater. Chem.*, 2011, **21**, 3422–3427.
147 S. Yang, X. Feng, L. Wang, K. Tang, J. Maier and K. Müllen, *Angew. Chem., Int. Ed.*, 2010, **49**, 4795–4799.
148 M. Jahan, Q. Bao and K. P. Loh, *J. Am. Chem. Soc.*, 2012, **134**, 6707–6713.
149 X. Yang, C. Cheng, Y. Wang, L. Qiu and D. Li, *Science*, 2013, **341**, 534–537.
150 P. Simon and Y. Gogotsi, *Acc. Chem. Res.*, 2012, **46**, 1094–1103.
151 S. Murali, N. Quarles, L. L. Zhang, J. R. Potts, Z. Tan, Y. Lu, Y. Zhu and R. S. Ruoff, *Nano Energy*, 2013, **2**, 764–768.
152 M. F. El-Kady, V. Strong, S. Dubin and R. B. Kaner, *Science*, 2012, **335**, 1326–1330.
153 V. Strong, S. Dubin, M. F. El-Kady, A. Lech, Y. Wang, B. H. Weiller and R. B. Kaner, *ACS Nano*, 2012, **6**, 1395–1403.
154 L. L. Zhang, X. Zhao, M. D. Stoller, Y. Zhu, H. Ji, S. Murali, Y. Wu, S. Perales, B. Clevenger and R. S. Ruoff, *Nano Lett.*, 2012, **12**, 1806–1812.
155 Y. Zhu, S. Murali, M. D. Stoller, K. J. Ganesh, W. Cai, P. J. Ferreira, A. Pirkle, R. M. Wallace, K. A. Cychosz, M. Thommes, D. Su, E. A. Stach and R. S. Ruoff, *Science*, 2011, **332**, 1537–1541.
156 L. Zhang, F. Zhang, X. Yang, G. Long, Y. Wu, T. Zhang, K. Leng, Y. Huang, Y. Ma, A. Yu and Y. Chen, *Sci. Rep.*, 2013, **3**, 1408.
157 C. Wu, X. Huang, G. Wang, L. Lv, G. Chen, G. Li and P. Jiang, *Adv. Funct. Mater.*, 2013, **23**, 506–513.
158 C.-M. Chen, Q. Zhang, C.-H. Huang, X.-C. Zhao, B.-S. Zhang, Q.-Q. Kong, M.-Z. Wang, Y.-G. Yang, R. Cai and D. Sheng Su, *Chem. Commun.*, 2012, **48**, 7149–7151.
159 K. Jiang, Q. Li and S. Fan, *Nature*, 2002, **419**, 801.
160 K. Koziol, J. Vilatela, A. Moisala, M. Motta, P. Cunniff, M. Sennett and A. Windle, *Science*, 2007, **318**, 1892–1895.
161 B. Vigolo, A. Pénicaud, C. Coulon, C. Sauder, R. Pailler, C. Journet, P. Bernier and P. Poulin, *Science*, 2000, **290**, 1331–1334.
162 Z. Xu, H. Y. Sun, X. L. Zhao and C. Gao, *Adv. Mater.*, 2013, **25**, 188–193.
163 Z. Xu and C. Gao, *Nat. Commun.*, 2011, **2**, 571.
164 H. P. Cong, X. C. Ren, P. Wang and S. H. Yu, *Sci. Rep.*, 2012, **2**, 613.
165 Z. L. Dong, C. C. Jiang, H. H. Cheng, Y. Zhao, G. Q. Shi, L. Jiang and L. T. Qu, *Adv. Mater.*, 2012, **24**, 1856–1861.
166 Z. Xu, Y. Zhang, P. G. Li and C. Gao, *ACS Nano*, 2012, **6**, 7103–7113.
167 Z. Xu, Z. Liu, H. Y. Sun and C. Gao, *Adv. Mater.*, 2013, **25**, 3249–3253.
168 Y. Zhao, C. Jiang, C. Hu, Z. Dong, J. Xue, Y. Meng, N. Zheng, P. Chen and L. Qu, *ACS Nano*, 2013, **7**, 2406–2412.
169 L. Chen, Y. L. He, S. G. Chai, H. Qiang, F. Chen and Q. Fu, *Nanoscale*, 2013, **5**, 5809–5815.
170 X. M. Li, T. S. Zhao, K. L. Wang, Y. Yang, J. Q. Wei, F. Y. Kang, D. H. Wu and H. W. Zhu, *Langmuir*, 2011, **27**, 12164–12171.
171 D. Li, J. T. McCann and Y. Xia, *Small*, 2005, **1**, 83–86.
172 Y. Zhao, X. Cao and L. Jiang, *J. Am. Chem. Soc.*, 2007, **129**, 764–765.
173 C. G. Hu, Y. Zhao, H. H. Cheng, Y. H. Wang, Z. L. Dong, C. C. Jiang, X. Q. Zhai, L. Jiang and L. T. Qu, *Nano Lett.*, 2012, **12**, 5879–5884.
174 M.-S. Wu and Y.-H. Fu, *Carbon*, 2013, **60**, 236–245.
175 J. Luo, X. Zhao, J. Wu, H. D. Jang, H. H. Kung and J. Huang, *J. Phys. Chem. Lett.*, 2012, **3**, 1824–1829.
176 K. H. Kim, M. Yang, K. M. Cho, Y.-S. Jun, S. B. Lee and H.-T. Jung, *Sci. Rep.*, 2013, **3**, 3251.
177 J. Luo, H. D. Jang, T. Sun, L. Xiao, Z. He, A. P. Katsoulidis, M. G. Kanatzidis, J. M. Gibson and J. Huang, *ACS Nano*, 2011, **5**, 8943–8949.
178 P. Guo, H. Song and X. Chen, *J. Mater. Chem.*, 2010, **20**, 4867–4874.
179 D. J. Han, J. H. Jung, J. S. Choi, Y. T. Kim and T. S. Seo, *Lab Chip*, 2013, **13**, 4006–4010.
180 J. Luo, H. D. Jang and J. Huang, *ACS Nano*, 2013, **7**, 1464–1471.
181 X. F. Ma, M. R. Zachariah and C. D. Zangmeister, *Nano Lett.*, 2012, **12**, 486–489.
182 Z. Yan, Y. Liu, J. Lin, Z. Peng, G. Wang, E. Pembroke, H. Zhou, C. Xiang, A.-R. O. Raji, E. L. G. Samuel, T. Yu, B. I. Yakobson and J. M. Tour, *J. Am. Chem. Soc.*, 2013, **135**, 10755–10762.
183 H. Wang, K. Sun, F. Tao, D. J. Stacchiola and Y. H. Hu, *Angew. Chem., Int. Ed.*, 2013, **52**, 9210–9214.
184 L. Qiu, J. Z. Liu, S. L. Y. Chang, Y. Wu and D. Li, *Nat. Commun.*, 2012, **3**, 1241.
185 H. Li, J. Wu, X. Qi, Q. He, C. Liusman, G. Lu, X. Zhou and H. Zhang, *Small*, 2013, **9**, 382–386.
186 F. Y. Zeng, Y. F. Kuang, Y. Wang, Z. Y. Huang, C. P. Fu and H. H. Zhou, *Adv. Mater.*, 2011, **23**, 4929–4932.
187 X. Xie, L. Ju, X. Feng, Y. Sun, R. Zhou, K. Liu, S. Fan, Q. Li and K. Jiang, *Nano Lett.*, 2009, **9**, 2565–2570.
188 F. Y. Zeng, Y. F. Kuang, G. Q. Liu, R. Liu, Z. Y. Huang, C. P. Fu and H. H. Zhou, *Nanoscale*, 2012, **4**, 3997–4001.
189 W. Zhou, J. Liu, T. Chen, K. S. Tan, X. Jia, Z. Luo, C. Cong, H. Yang, C. M. Li and T. Yu, *Phys. Chem. Chem. Phys.*, 2011, **13**, 14462–14465.
190 L. M. Viculis, J. J. Mack and R. B. Kaner, *Science*, 2003, **299**, 1361.
191 J. Zheng, H. Liu, B. Wu, Y. Guo, T. Wu, G. Yu, Y. Liu and D. Zhu, *Adv. Mater.*, 2011, **23**, 2460–2463.
192 Y. Chen, F. Guo, Y. Qiu, H. Hu, I. Kulaots, E. Walsh and R. H. Hurt, *ACS Nano*, 2013, **7**, 3744–3753.
193 Y. Chen, F. Guo, A. Jachak, S.-P. Kim, D. Datta, J. Liu, I. Kulaots, C. Vaslet, H. D. Jang, J. Huang, A. Kane, V. B. Shenoy and R. H. Hurt, *Nano Lett.*, 2012, **12**, 1996–2002.
194 Y. Tian, G. Wu, X. Tian, X. Tao and W. Chen, *Sci. Rep.*, 2013, **3**, 3327.
195 X. Li, X. Wang, L. Zhang, S. Lee and H. Dai, *Science*, 2008, **319**, 1229–1232.
196 S. Yin, Y. Goldovsky, M. Herzberg, L. Liu, H. Sun, Y. Zhang, F. Meng, X. Cao, D. D. Sun, H. Chen, A. Kushmaro and X. Chen, *Adv. Funct. Mater.*, 2013, **23**, 2972–2978.

197 S. H. Lee, H. W. Kim, J. O. Hwang, W. J. Lee, J. Kwon, C. W. Bielawski, R. S. Ruoff and S. O. Kim, *Angew. Chem., Int. Ed.*, 2010, **49**, 10084–10088.
198 C.-M. Chen, Q. Zhang, X.-C. Zhao, B. Zhang, Q.-Q. Kong, M.-G. Yang, Q.-H. Yang, M.-Z. Wang, Y.-G. Yang, R. Schlogl and D. S. Su, *J. Mater. Chem.*, 2012, **22**, 14076–14084.
199 P. Simon and Y. Gogotsi, *Nat. Mater.*, 2008, **7**, 845–854.
200 S. W. Lee, B. M. Gallant, H. R. Byon, P. T. Hammond and Y. Shao-Horn, *Energy Environ. Sci.*, 2011, **4**, 1972–1985.
201 L. L. Zhang and X. S. Zhao, *Chem. Soc. Rev.*, 2009, **38**, 2520–2531.
202 G. Wang, L. Zhang and J. Zhang, *Chem. Soc. Rev.*, 2012, **41**, 797–828.
203 Y. Huang, J. Liang and Y. Chen, *Small*, 2012, **8**, 1805–1834.
204 M. D. Stoller, S. Park, Y. Zhu, J. An and R. S. Ruoff, *Nano Lett.*, 2008, **8**, 3498–3502.
205 C. Liu, Z. Yu, D. Neff, A. Zhamu and B. Z. Jang, *Nano Lett.*, 2010, **10**, 4863–4868.
206 Y. Wang, Z. Shi, Y. Huang, Y. Ma, C. Wang, M. Chen and Y. Chen, *J. Phys. Chem. C*, 2009, **113**, 13103–13107.
207 L. L. Zhang, R. Zhou and X. S. Zhao, *J. Mater. Chem.*, 2010, **20**, 5983–5992.
208 Y. P. Zhai, Y. Q. Dou, D. Y. Zhao, P. F. Fulvio, R. T. Mayes and S. Dai, *Adv. Mater.*, 2011, **23**, 4828–4850.
209 S. Bose, T. Kuila, A. K. Mishra, R. Rajasekar, N. H. Kim and J. H. Lee, *J. Mater. Chem.*, 2012, **22**, 767–784.
210 A. Ghosh and Y. H. Lee, *ChemSusChem*, 2012, **5**, 480–499.
211 M. J. Zhi, C. C. Xiang, J. T. Li, M. Li and N. Q. Wu, *Nanoscale*, 2013, **5**, 72–88.
212 Z.-S. Wu, Y. Sun, Y.-Z. Tan, S. Yang, X. Feng and K. Müllen, *J. Am. Chem. Soc.*, 2012, **134**, 19532–19535.
213 W.-Y. Tsai, R. Lin, S. Murali, L. Li Zhang, J. K. McDonough, R. S. Ruoff, P.-L. Taberna, Y. Gogotsi and P. Simon, *Nano Energy*, 2013, **2**, 403–411.
214 Y. Wang, Y. Wu, Y. Huang, F. Zhang, X. Yang, Y. Ma and Y. Chen, *J. Phys. Chem. C*, 2011, **115**, 23192–23197.
215 J. Xia, F. Chen, J. Li and N. Tao, *Nat. Nanotechnol.*, 2009, **4**, 505–509.
216 H. Jiang, P. S. Lee and C. Li, *Energy Environ. Sci.*, 2013, **6**, 41–53.
217 R. Ramachandran, V. Mani, S. M. Chen, R. Saraswathi and B. S. Lou, *Int. J. Electrochem. Sci.*, 2013, **8**, 11680–11694.
218 Y. He, W. Chen, C. Gao, J. Zhou, X. Li and E. Xie, *Nanoscale*, 2013, **5**, 8799–8820.
219 H. Wang, H. S. Casalongue, Y. Liang and H. Dai, *J. Am. Chem. Soc.*, 2010, **132**, 7472–7477.
220 Y. He, W. Chen, X. Li, Z. Zhang, J. Fu, C. Zhao and E. Xie, *ACS Nano*, 2012, **7**, 174–182.
221 J. Ji, L. L. Zhang, H. Ji, Y. Li, X. Zhao, X. Bai, X. Fan, F. Zhang and R. S. Ruoff, *ACS Nano*, 2013, **7**, 6237–6243.
222 L. Hu, M. Pasta, F. L. Mantia, L. Cui, S. Jeong, H. D. Deshazer, J. W. Choi, S. M. Han and Y. Cui, *Nano Lett.*, 2010, **10**, 708–714.
223 H. H. Cheng, Z. L. Dong, C. G. Hu, Y. Zhao, Y. Hu, L. T. Qu, N. Chena and L. M. Dai, *Nanoscale*, 2013, **5**, 3428–3434.
224 Y. Xu, Z. Lin, X. Huang, Y. Liu, Y. Huang and X. Duan, *ACS Nano*, 2013, **7**, 4042–4049.
225 Y. Fu, X. Cai, H. Wu, Z. Lv, S. Hou, M. Peng, X. Yu and D. Zou, *Adv. Mater.*, 2012, **24**, 5713–5718.
226 J. Bae, Y. J. Park, M. Lee, S. N. Cha, Y. J. Choi, C. S. Lee, J. M. Kim and Z. L. Wang, *Adv. Mater.*, 2011, **23**, 3446–3449.
227 J. Bae, M. K. Song, Y. J. Park, J. M. Kim, M. Liu and Z. L. Wang, *Angew. Chem., Int. Ed.*, 2011, **50**, 1683–1687.
228 J. Ren, L. Li, C. Chen, X. Chen, Z. Cai, L. Qiu, Y. Wang, X. Zhu and H. Peng, *Adv. Mater.*, 2013, **25**, 1155–1159.
229 K. Wang, Q. Meng, Y. Zhang, Z. Wei and M. Miao, *Adv. Mater.*, 2013, **25**, 1494–1498.
230 Y. Cao, M. Zhu, P. Li, R. Zhang, X. Li, Q. Gong, K. Wang, M. Zhong, D. Wu, F. Lin and H. Zhu, *Phys. Chem. Chem. Phys.*, 2013, **15**, 19550–19556.
231 Y. Li, K. Sheng, W. Yuan and G. Shi, *Chem. Commun.*, 2013, **49**, 291–293.
232 B.-H. Kim, K. S. Yang and J. P. Ferraris, *Electrochim. Acta*, 2012, **75**, 325–331.
233 X. Li, X. Zang, Z. Li, X. Li, P. Li, P. Sun, X. Lee, R. Zhang, Z. Huang, K. Wang, D. Wu, F. Kang and H. Zhu, *Adv. Funct. Mater.*, 2013, **23**, 4862–4869.
234 T. Huang, B. Zheng, L. Kou, K. Gopalsamy, Z. Xu, C. Gao, Y. Meng and Z. Wei, *RSC Adv.*, 2013, **3**, 23957–23962.
235 X. Li, T. Zhao, Q. Chen, P. Li, K. Wang, M. Zhong, J. Wei, D. Wu, B. Wei and H. Zhu, *Phys. Chem. Chem. Phys.*, 2013, **15**, 17752–17757.
236 Z. Zeng, X. Huang, Z. Yin, H. Li, Y. Chen, H. Li, Q. Zhang, J. Ma, F. Boey and H. Zhang, *Adv. Mater.*, 2012, **24**, 4138–4142.
237 X. Wang, L. Jiao, K. Sheng, C. Li, L. Dai and G. Shi, *Sci. Rep.*, 2013, **3**, 1996.
238 Y. Fang, Y. Lv, R. Che, H. Wu, X. Zhang, D. Gu, G. Zheng and D. Zhao, *J. Am. Chem. Soc.*, 2013, **135**, 1524–1530.
239 T. H. Han, Y. K. Huang, A. T. L. Tan, V. P. Dravid and J. X. Huang, *J. Am. Chem. Soc.*, 2011, **133**, 15264–15267.
240 M. Chhowalla, H. S. Shin, G. Eda, L.-J. Li, K. P. Loh and H. Zhang, *Nat. Chem.*, 2013, **5**, 263–275.
241 X. Huang, Z. Zeng, S. Bao, M. Wang, X. Qi, Z. Fan and H. Zhang, *Nat. Commun.*, 2013, **4**, 1444.
242 X. Huang, Z. Zeng and H. Zhang, *Chem. Soc. Rev.*, 2013, **42**, 1934–1946.
243 C. Zhu, Z. Zeng, H. Li, F. Li, C. Fan and H. Zhang, *J. Am. Chem. Soc.*, 2013, **135**, 5998–6001.
244 Z. Zeng, C. Tan, X. Huang, S. Mao and H. Zhang, *Energy Environ. Sci.*, 2014, **7**, 797–803.
245 H. Li, J. Wu, X. Huang, G. Lu, J. Yang, X. Lu, Q. Xiong and H. Zhang, *ACS Nano*, 2013, **7**, 10344–10353.
246 H. Li, G. Lu, Y. Wang, Z. Yin, C. Cong, Q. He, L. Wang, F. Ding, T. Yu and H. Zhang, *Small*, 2013, **9**, 1974–1981.
247 J. Wu, H. Li, Z. Yin, H. Li, J. Liu, X. Cao, Q. Zhang and H. Zhang, *Small*, 2013, **9**, 3314–3319.
248 Q. H. Wang, K. Kalantar-Zadeh, A. Kis, J. N. Coleman and M. S. Strano, *Nat. Nanotechnol.*, 2012, **7**, 699–712.